NCS1 regulates Ca^{2+}-Dependent Focal Exocytosis of Golgi-derived Vesicles to Help Phagocytic uptake in Macrophages

Nimi Vashi[1], Syed Bilal Ahmad Andrabi[$,1], Swapnil Ghanwat[$,1], Mrutyunjay Suar[2] and Dhiraj Kumar*[,1]

[1]Cellular Immunology Group, International Centre for Genetic Engineering and Biotechnology, Aruna Asaf Ali Marg, New Delhi-110067, India

and

[2]School of Biotechnology, KIIT University, Bhubaneswar-751024, India

Running title: *Role of Golgi-derived vesicles in phagocytosis*

[$] Equal contribution

***Correspondence:** dhiraj@icgeb.res.in
Phone: +91-11-26742357
Fax: +91-11-26742316

Abstract

During phagocytic uptake by macrophages, role of Golgi apparatus or vesicles derived from it has never been established. Using fluorescently tagged Mannosidase-II, a marker for Golgi-derived vesicles, we show these vesicles are recruited during uptake of diverse targets including latex beads, *E. coli*, *Salmonella* Typhimurium and *Mycobacterium tuberculosis* in both human and mouse macrophages. The recruitment of Mannosidase-II vesicles occurred very early during phagocytosis, which was mediated by focal exocytosis. The focal movement of Mannosidase-II vesicles required Ca^{2+} from both extra- and intra-cellular sources apart from PI3Kinase, microtubules and dynamin-2. At the site of uptake voltage-gated Ca^{2+} channels help establish a Ca^{2+}-dependent local PIP3 gradient, which guide the focal movement. Mannosidase-II vesicles also contained Neuronal Calcium Sensor-1 (NCS1) and resembled secretory vesicles. Depleting NCS1 blocked the recruitment of Mannosidase-II vesicles and inhibited phagocytic uptake of diverse targets. We propose Golgi-derived vesicles provide membrane for phagosome biogenesis and are universally required for phagocytosis, the key innate defense function.

Introduction

Phagocytosis lies at the core of innate defense mechanisms in higher eukaryotes. The process of phagocytosis involves internalization of external particles including pathogens, cellular debris etc. into a specialized membrane bound organelle called phagosomes. The phagosome thus formed undergoes a series of fusion and fission events leading to acquisition of hydrolytic enzymes and microbicidal properties to mature into phago-lysosomes (Aderem and Underhill, 1999; Flannagan et al., 2012; Jutras and Desjardins, 2005).

It was perceived initially that the membrane for phagosomes could be solely derived from the plasma membrane (Cannon and Swanson, 1992). However in macrophages, the professional phagocytes, which can engulf objects bigger than their own size without significantly altering their function, there is no apparent decline in the membrane surface area following phagocytosis(Holevinsky and Nelson, 1998). Rather capacitance measurement experiments showed that a concomitant increase in the membrane surface area precedes resealing of the phagosome, suggesting supply of phagosome membrane from intracellular sources(Holevinsky and Nelson, 1998). Professional phagocytes are therefore expected to be under tremendous pressure to sustain the supply of the membrane so as to effectively phagocytize their targets. Consequently a variety of membrane bound organelles including the vesicles originating from recycling endosomes and lysosomes as well as ER were later shown to provide membrane for the nascent phagosome(Bajno et al., 2000; Gagnon et al., 2002; Tardieux et al., 1992).

Vesicle recruitment during phagocytosis involves exocytosis of vesicles in the vicinity of nascent phagosomes (Braun and Niedergang, 2006). Studies in the past have shown secretion of vesicular contents like lysosomal hydrolases and azurophil

granules during engulfment by macrophages and neutrophils respectively, thereby coupling the process of phagocytosis with targeted exocytosis, a process also termed as focal exocytosis (Bajno et al., 2000; Braun and Niedergang, 2006). Recycling endosome marker VAMP3, a soluble N-ethylmaleimide-sensitive factor attachment protein receptor proteins on vesicles (v-SNARE), was shown to accumulate at the early phagosomes through focal exocytosis (Bajno et al., 2000). Moreover Synaptotagmin V (SytV), a Ca^{2+} sensor on the recycling endosomes was shown to regulate phagocytosis but not phagosome maturation, suggesting a key role of Ca^{2+} in the regulation of vesicle exocytosis (Vinet et al., 2008). Similarly SytVII, a lysosome resident Ca^{2+} sensor was reported to regulate delivery of lysosome membrane to the nascent phagosomes (Czibener et al., 2006). Interestingly, SytVII was also shown to regulate Ca^{2+} dependent exocytosis of lysosomes during plasma membrane repair (Reddy et al., 2001). Recently TRPML1, a key Ca^{2+} channel in the lysosomes was shown to regulate focal exocytosis during phagocytosis of large particles (Samie et al., 2013). Phosphoinositide3kinase (PI3K) is yet another key regulator of phagocytosis, and is believed to help pseudopod extension around the particles during phagocytosis (Cox et al., 1999). However, inhibition of PI3K by wortmannin may not limit membrane availability for phagocytosis (Cox et al., 1999). There are some reports however suggesting the role of PI3K in recruiting the membranes from intracellular sources (Underhill and Ozinsky, 2002). Yet another study revealed recruitment of endoplasmic reticulum (ER) at the site of phagocytosis to provide membrane for the newly formed phagosomes, a process that was regulated by the ER resident SNARE protein ERS24 (Gagnon et al., 2002; Jutras and Desjardins, 2005).

Intriguingly, despite being intricately involved with the recycling endocytic network and as one of the major sources of vesicles destined to the plasma membrane like

97 secretory vesicles, involvement of Golgi Apparatus (GA) or vesicles derived from GA
98 in the process of phagocytosis has been ruled out (Becker et al., 2005). However in an
99 interesting observation, fragmentation and reorganization of GA was reported during
100 a process of frustrated phagocytosis (Bainton et al., 1989). Interestingly majority of
101 the reports that conclude no direct involvement of GA during phagocytic uptake
102 relied on the experiments that were limited to Fcγ-Receptor mediated phagocytosis
103 (Beemiller et al., 2006; Braun et al., 2007; Zhang et al., 1998). Here we studied the
104 role of vesicles derived from the GA during phagocytic uptake. Mannosidase-II, a
105 medial and trans-Golgi marker was also detected within secretory granules and at the
106 surface of certain cell types like enterocytes, pancreatic acinar cells and goblet cells
107 (Velasco et al., 1993). Later, using Mannosidase-II as the marker of Golgi-derived
108 vesicles its recruitment to cell surface was used to track the role of these vesicles
109 during plasma membrane repair in mouse bone marrow derived primary macrophages
110 (Divangahi et al., 2009; Velasco et al., 1993). Here we show, Mannosidase-II
111 containing Golgi-derived vesicles are recruited during phagocytosis of a variety of
112 targets including inert particles (latex beads), non-pathogenic bacteria (*E. coli*) and
113 pathogenic bacteria (*Salmonella* Typhimurium and *Mycobacterium tuberculosis*) in
114 mouse (RAW264.7 and BMDMs) and human (THP-1 and U937) macrophages. The
115 recruitment of Mannosidase-II vesicles at the site of phagocytosis occurred through
116 the process of focal exocytosis. This process was dependent on voltage-gated Ca^{2+}
117 channels that helped establish a Ca^{2+} dependent PIP3 gradient for uptake.
118 Mechanistically, TGN and secretory vesicle resident protein NCS1 sensed and
119 triggered the movement of vesicles to help phagosome biogenesis.
120

Results

α-Mannosidase-II (MAN2A) localizes to Golgi Apparatus (GA) and Golgi derived vesicles

To confirm the localization of Mannosidase-II to GA in our experimental set-up, we nucleofected THP-1 human macrophages and RAW264.7 mouse macrophages with a mCherry-tagged Mannosidase-II construct [mCherry-MannII-N-10 (mCherry-MAN2A), Addgene plasmid # 55074] and visualized the cells under Nikon A1R confocal microscope (see methods). Expression of Mannosidase-II in these cells distinctly labeled the GA as shown in figure 1A. We also immuno-stained Mannosidase-II using specific antibody, which labeled the GA (Fig. 1B). Treatment of mCherry-MAN2A expressing cells with Brefeldin A, the classical inhibitor of Golgi function, resulted in the disruption and fragmentation of the GA structure (Fig 1C). In both transfected as well as antibody stained cells, in addition to the main GA we could also observe several smaller punctate structures, representing the Golgi-derived vesicles (Fig. 1A and B). In U937 cells stably expressing mRuby-tagged Beta-1,4-Galactosyltransferase (B4GALT1-mRuby), a mid-Golgi resident enzyme, no such vesicle like structures could be seen (Fig. 1D), Mannosidase-II however co-localized with B4GALT1-mRuby (Fig. 1D). These results confirmed that the Mannosidase-II construct used in this study labeled GA and Golgi-derived vesicles.

Mannosidase-II is recruited at the site of phagocytic uptake

RAW264.7 cells transfected with mCherry tagged Mannosidase-II were incubated with mouse-IgG coated latex beads (see methods) that were either unstained or stained with anti-mouse IgG-Alexa488. At 30 minutes and one-hour post-addition of beads to the macrophages, cells were fixed and visualized under the microscope. We observed the recruitment of Mannosidase-II to the sites where latex beads were

146 phagocytosed, forming ring like structure around the beads at many instances (Fig.
147 2A and Fig. S1A). Overall intensity of Mannosidase-II at the bead surface had a
148 median of ~900 at 30 minutes and ~1500 arbitrary units (A.U.) at 1 hour as
149 determined using the 3-D module tool in Imaris 7.2 (see methods, Fig 2A). To check
150 whether Mannosidase-II recruitment during phagocytosis was a general phenomenon
151 we also monitored uptake of non-pathogenic bacterium *E. coli* and pathogenic
152 bacteria *Salmonella* Typhimurium. In both the cases, we could see Mannosidase-II
153 recruited at very early stages of phagocytosis. In the case of *E. coli,* nearly 60% of the
154 bacteria at the site of entry showed Mannosidase-II recruitment at 15 and 30 minutes
155 post-infection while nearly 30% of *Salmonella* containing phagosomes showed
156 Mannosidase-II recruitment at 5 and 10 minutes (Fig 2B). In the case of yet another
157 pathogenic bacteria *Mycobacterium tuberculosis* strain H37Rv, Mannosidase-II was
158 recruited at 30-40% phagosomes at the time of entry (Fig. 2C). Recruitment of
159 Mannosidase-II at the early phagosomes in case of H37Rv was also verified by
160 immuno-staining against Mannosidase-II (Fig. S1B). To confirm that the
161 Mannosidase-II positive phagosomes indeed represented early stages of phagosomes,
162 we immuno-stained the mCherry-MAN2A expressing cells, that were either incubated
163 with mouse-IgG coated latex beads or infected with *Mtb*, with anti-transferrin
164 receptor (TfR) antibody. We observed significant overlap between recruited
165 Mannosidase-II and TfR around the internalized beads and *Mtb* (Fig. 2D and 2E). TfR
166 recruitment around phagocytized beads showed saturating levels with median of
167 around 4095 A.U., much higher than the intensity distribution of Mannosidase-II
168 (~1000 A.U., Fig. 2D). In case of *Mtb* too, TfR showed relatively higher co-
169 localization with the phagosomes (~40-60%) compared to Mannosidase-II (30-50%,
170 Fig. 2E). Expectedly, TfR on *Mtb* phagosomes declined rapidly from one-hour post

infection to two hours post infection (Fig. 2E). To further establish that the membrane recruitment of Mannosidase-II during phagocytosis was an early event, we took U937 cells that stably expressed EGFP fused with a plasma membrane targeting sequence from Neuromodulin (Liu et al., 1991). We nucleofected these cells with mCherry-MAN2A followed by incubation with the latex beads. As shown in figure 2F, Mannosidase-II was recruited at the site of phagocytosis where it mostly localized to the cytosolic face of the newly forming phagosome while the latex beads were still getting internalized. We also verified the recruitment of Mannosidase-II in mouse bone marrow derived macrophages (BMDMs) during phagocytic uptake of *E. coli*, thus ensuring that it was not a phenomenon restricted to only cell-lines (Fig. S1C).

Characterization of early phagosomes reveals direct involvement of secretory vesicles derived from the GA in the phagosome biogenesis

As shown above and by others (Divangahi et al., 2009; Velasco et al., 1993), Mannosidase-II marks both GA and Golgi-derived vesicles. In most of the fields observed in the previous sections, we could see Mannosidase-II organized into a separate Golgi structure, underscoring the fact that the phagosome associated Mannosidase-II were derived from the recruitment of Golgi-derived vesicles at the site of infection. To further confirm the selective enrichment of Mannosidase-II at the nascent phagosomes, we purified latex beads phagosomes using sucrose density gradient ultra-centrifugation from macrophages within 1 hour of uptake (Fig. 3A). The phagosome preparation showed presence of expected early phagosome markers like TfR and RAB5 (Fig. 3B). They also showed presence of previously reported markers like VAMP3 from recycling endosomes and Calnexin from ER (Fig. 3B). At the same time, the phagosome preparation was devoid of any mitochondrial, nuclear or cytosolic contamination (Fig. 3B). In agreement with the microscopy data,

196 phagosomes also showed presence of Mannosidase-II, the marker for Golgi-derived
197 vesicles (Fig. 3B). In addition, we could also score the presence of another Golgi-
198 derived secretory vesicles marker NCS1 in the phagosomes (Fig. 3B). We verified
199 that there was no GA contamination in the preparation as the phagosomes were
200 devoid of B4GALT1 (Fig. 3B).
201 Trafficking of vesicles in the cells is regulated by a large number of proteins
202 including small GTPases like RABs, ADP-Ribosylation factors (ARFs) and SNAREs
203 (Chen and Scheller, 2001; Gillingham and Munro, 2007; Stenmark, 2009). In order to
204 understand which RABs, SNAREs or ARFs could be involved in the recruitment of
205 Mannosidase-II vesicles at the phagosomes we performed mass-spectrometry of the
206 purified latex beads phagosome preparations, specifically to identify molecules below
207 25kDa molecular weight (Fig. S2, see methods). We were able to identify about 290
208 proteins from this preparation, all of them below 25kDa molecular weight
209 (Supplementary table S1). We performed a gene ontology analysis on these proteins
210 using Amigo2.0 database to specifically see enrichment of eleven classes including
211 ER, GA, secretory vesicles, recycling endosomes, endocytic vesicles,
212 neurotransmitter release, TGN, vesicle mediated transport, phagocytosis/engulfment,
213 exocytosis and endosomal transport (Fig. 3C, Supplementary table S2). A large
214 number of proteins belonging to ER were found in the phagosomes (Fig. 3C). The
215 phagosome mass spectrometry data revealed presence of 17 different RABs, 5 out of
216 6 known ARFs and four VAMPs. Many of these proteins are involved with Golgi
217 apparatus, exocytosis, secretory vesicles and neurotransmitter release (Fig. 3C).
218 VAMP2 gets enriched in the secretory vesicles that are released from the GA and
219 targeted to the membranes (Faurschou and Borregaard, 2003). It also helps in the
220 release of neurotransmitters by regulating the exocytosis of secretory vesicles (Shen et

al., 2015). Presence of a large variety of proteins that could regulate vesicle trafficking on the early phagosomes could potentially mean a complex interplay of different vesicle trafficking pathways in the process of phagosome biogenesis. Since the role of vesicles derived from recycling endosomes and involvement of ER was already established during phagosome biogenesis, presence of markers associated with vesicles derived from the GA reconfirmed the utility of this organelle as an additional source of membranes for phagosome biogenesis.

Mannosidase-II positive Golgi-derived vesicles are recruited at the phagosomes through focal exocytosis

We next wanted to understand how Mannosidase-II vesicle recruitment was regulated during phagocytosis. It was previously reported that Mannosidase-II positive Golgi-derived vesicles get recruited at the site of membrane damage during repair (Divangahi et al., 2009). It is also well established that vesicular movement during membrane repair occurs through focal exocytosis (Reddy et al., 2001). To verify the recruitment of Mannosidase-II during membrane repair, we treated RAW264.7 macrophages expressing mCherry-MAN2A with detergent for 15 minutes to cause membrane damage. The cells were then followed live for next 2-3 hours to assess recruitment of Mannosidase-II at the damaged site. We could observe formation of membrane lesion upon detergent treatment and subsequent recruitment of Mannosidase-II that eventually sealed the lesion (Fig. S3) thereby highlighting the targeted exocytic movement of Mannosidase-II vesicles.

One of the key regulators of focal exocytosis, specifically for post-Golgi transport vesicles towards the plasma membrane, is dynamin (Kreitzer et al., 2000). Dynamins are the member of large GTPase family and dynamin-2 is the ubiquitously expressed isoform while dynamin-1 is mostly neuronal (Henley and McNiven, 1996; Warnock

et al., 1997). Their involvement in budding of transport vesicles from the Golgi is also well documented along with their role in regulating focal exocytosis (Praefcke and McMahon, 2004; Samie et al., 2013). In mCherry-MAN2A expressing RAW264.7 cells, we observed significant overlap of Mannosidase-II with dynamin-2 on the phagosomes containing either latex beads or *Mtb* (Fig. 4A and 4B). Again as in the case of TfR, dynamin-2 recruitment on the nascent phagosomes was relatively higher than Mannosidase-II recruitment for both latex beads and *Mtb* (Fig. 4A and 4B). Presence of dynamin-2 at the phagosomes was consistent with previous reports, which showed their recruitment at early phagosomes during phagocytosis (Gold et al., 1999).

We next inhibited dynamin-2 by dynasore treatment for varying period of time and observed its effect on Mannosidase-II recruitment and phagocytosis. In the case of latex beads, four hours of pre-treatment with dynasore (at 40 and 80μM) resulted in a significant inhibition in the recruitment of Mannosidase-II at the phagosomes (Fig. 4C). It also markedly reduced the phagocytosis of latex beads (Fig. 4D). Dynasore treatment also inhibited uptake of *Mtb* in THP-1 macrophages (Fig. S4A). There was noticeable decline in the recruitment of Mannosidase-II at the *Mtb* phagosomes (Fig. S4B). Dynamin assisted movement of vesicles also require microtubules (Kreitzer et al., 2000). Inhibition of microtubules by nocodazole treatment resulted in a transient decline in the uptake of *Mtb* and latex beads (Fig. S4C and D). Further, nocodazole treatment resulted in a marked decline in the recruitment of Mannosidase-II to the phagosomes containing latex beads and *Mtb* (Fig. S4E and F). These results established that the Mannosidase-II positive Golgi-derived vesicles were recruited at the phagosomes through focal exocytosis and were assisted by dynamins.

Golgi-derived vesicles co-operate with the vesicles derived from the recycling endosomes during phagocytosis

Recruitment of vesicles from endocytic origin (VAMP3 positive) and lysosomal origin (LAMP1 positive) during phagocytosis has been reported earlier (Bajno et al., 2000; Czibener et al., 2006). We also observed presence of VAMP3 on the early latex beads phagosomes as shown above (Fig. 3B). This finding was reconfirmed in mCherry-MAN2A expressing RAW264.7 cells, where both latex beads and *Mtb* very early during phagocytosis (30 minutes and 1 hour for beads; 1 hour and 2 hours for *Mtb*) showed very high recruitment of and co-localization with VAMP-3 (Fig. 4E and F). In case of *Mtb*, more than 90% of the Mannosidase-II positive phagosomes were also positive for VAMP-3 (Fig. 4F). Overall, VAMP-3 recruitment was much higher compared to Mannosidase-II recruitment at the site of phagocytosis (Fig. 4E and F). Thus spatially and temporally, Mannosidase-II recruitment at the phagosomes was strikingly similar to VAMP3 recruitment. Moreover similar to the case of Golgi-derived vesicles here, the recruitment of VAMP-3 positive vesicles from the recycling endosomes is also dependent on focal exocytosis (Bajno et al., 2000). Thus it is very likely that vesicles from different origins co-operate in aiding the biogenesis of phagosomes.

Phosohatidylinositol3Kinase (PI3K) is required for Mannosidase-II recruitment at the nascent phagosomes and phagocytosis

The role of PI3K in regulating phagocytosis is well known where its function is believed to be mostly required for pseudopod extension around the cargo during phagocytosis (Cox et al., 1999). We wanted to test whether some of the effects of PI3K on phagocytosis were due to its involvement in the recruitment of Mannosidase-II vesicles for phagocytosis. Inhibition of PI3K by wortmannin led to nearly 80%

295 decline in the uptake of latex beads at 30 and 60 minutes (Fig. 5A). In case of *Mtb*,
296 the decline in uptake was ~85% at 1 and 2 hours post-infection and 70% at 4 hours
297 post-infection (Fig. 5B). In the case of *Mtb* we assayed multiple doses of wortmannin
298 and three different MOIs (Fig. S5A). The effect of wortmannin on the uptake of *Mtb*
299 was dependent on the inhibitor concentration however independent of the MOIs used
300 (Fig. S5A). Wortmannin was equally effective in inhibiting the phagocytic uptake of
301 *Salmonella* Typhimurium in THP-1 macrophages (Fig. S5B). Curiously, PI3K
302 inhibition also resulted in a marked decrease in the recruitment of Mannosidase-II at
303 the nascent phagosomes (Fig. 5C and D). Thus at least to some extent, it seems the
304 effect of inhibition of PI3K on phagocytosis may be due to a reduced recruitment of
305 Mannosidase-II positive Golgi-derived vesicles at the phagosomes. Similar effect of
306 PI3K inhibition on the membrane recruitment for the newly forming phagosomes has
307 been discussed previously (Underhill and Ozinsky, 2002).

308 **Extracellular Calcium (Ca^{2+}) is needed for phagocytosis and focal exocytosis of**
309 **Golgi-derived vesicles at the site of phagocytosis**

310 We next wanted to understand the immediate early mediators of focal exocytosis
311 during phagocytosis. Focal exocytosis of vesicles derived from the recycling
312 endosomes as well as lysosomes depends on the functioning of key Ca^{2+} sensors in
313 these compartments (Czibener et al., 2006; Samie et al., 2013; Vinet et al., 2008). It
314 was therefore imperative to test the role of Ca^{2+} in the focal movement of Golgi-
315 derived vesicles. Release of Ca^{2+} from intracellular stores is one of the key signaling
316 events during the course of phagocytosis and downstream maturation of the
317 phagosomes (Koul et al., 2004). Expectedly, phagocytosis of both latex beads and
318 H37Rv in THP-1 macrophages was severely hampered in the presence of TMB-8
319 (Fig. 5E and F), an inhibitor of the IP3 receptor that serves as the Ca^{2+} release channel

from intracellular stores like ER upon binding with IP3 (Singh et al., 2005). Intriguingly, presence of Ca^{2+} chelator EGTA in the extracellular media also inhibited phagocytic uptake of both latex beads and H37Rv in THP-1 macrophages (Fig. 5E and F) thereby suggesting the involvement of extracellular Ca^{2+} in the phagocytic uptake. However it could simply imply the effect of capacitative Ca^{2+} influx, which typically requires the CRAC channels and happens immediately after the intracellular stores are exhausted of Ca^{2+} (Singh et al., 2005). Treatment with both TMB-8 and EGTA had additive effect on the uptake of latex beads but not on the uptake of *Mtb* by THP-1 macrophages (Fig. 5E and F). We also noted a much more pronounced and sustained effect of TMB-8 and EGTA+TMB8 (~70% and ~85% inhibition respectively, Fig. 5E) on the uptake of latex beads as against that of *Mtb* (~25% and ~45% inhibition respectively, Fig. 5F). As observed in the case of wortmannin treatment, inhibition of Ca^{2+} signaling also resulted in a marked decline in the recruitment of Mannosidase-II at the nascent phagosomes (Fig. 5C and D).

Entry of extracellular Ca^{2+} through voltage-gated Ca^{2+} channels helps create the foci for the recruitment of vesicles during phagocytosis

The role and mechanism of recruitment of extracellular Ca^{2+} during phagocytosis is limited to the capacitative influx (Lee et al., 2003) or through passive accumulation of Ca^{2+} in the phagosomes during phagocytosis (Lundqvist-Gustafsson et al., 2000). An increase in the local Ca^{2+} concentration around phagosomes has been reported to facilitate phagocytosis (Stendahl et al., 1994). Interestingly, the role of extracellular Ca^{2+} during membrane repair process and focal exocytosis of vesicles to the damaged site has been extensively reported (Miyake and McNeil, 1995; Steinhardt et al., 1994; Togo et al., 1999). Similarly during neurotransmitter release in the neuronal cells, activation of voltage-gated Ca^{2+} channels during action potential helps focal

345 exocytosis of secretory vesicles (Sudhof, 2012). We hypothesized that one of the
346 earliest signals during phagocytic uptake could consist of Ca^{2+} entry into the cells
347 through the voltage-gated Ca^{2+} channel. In THP-1 macrophages treated with
348 loperamide hydrochloride or amlodipine besylate (inhibitors of L/P-type and L –type
349 voltage gated Ca^{2+} channels respectively) (Church et al., 1994; Kochegarov, 2003),
350 phagocytosis of *E. coli* declined considerably (Fig. 6A). These treatments were also
351 effective against phagocytosis of *Mtb* and latex beads in THP-1 macrophages (Fig.
352 S6A and B). Treatment with any of these two inhibitors also blocked Mannosidase-II
353 recruitment at the nascent phagosomes during uptake of latex beads in THP-1
354 macrophages (Fig. 6B). Thus voltage-gated channel seems to play an important role
355 during phagocytosis of diverse targets.
356 We next wanted to understand whether extracellular Ca^{2+} helped decide the foci for
357 the recruitment of Golgi-derived vesicles during phagosome formation (Sudhof,
358 2012). We investigated the accumulation of PIP3 at the site of engulfment. Inhibition
359 of PIP3 by wortmannin treatment abrogates the uptake as observed in this study (Fig.
360 5) as well as reported earlier (Cox et al., 1999). PIP3 is known to interact with the
361 Pleckstrin Homology (PH) domain of proteins. In cells expressing AKT-PH domain
362 fused with mCherry (AKT-PH-mCherry), at 5 minutes post-addition of *E. coli*, we
363 observed, expectedly, a significant accumulation of PIP3 at the site of bacterial entry
364 (Fig. 6C). Also there was a gradual decline in the PIP3 levels as we move further into
365 the cells from the site of phagocytosis (Fig. 6C). However in cells pre-treated with the
366 Ca^{2+} chelator (EGTA, 3mM), the selective accumulation of PIP3 at the site of
367 phagocytosis was lost (Fig. 6C) and PIP3 was almost uniformly distributed across the
368 cell irrespective of the site of engagement with the bacteria (Fig. 6C). Surprisingly,
369 similar effect on PIP3 distribution was observed when these cells were pre-treated

with either loperamide or amlodipine (Fig. 6C). In both these cases, the distribution of PIP3 in the cells was not influenced by the site of engagement with the bacteria (Fig. 6C). In cells treated with the PI3K inhibitor wortmannin, AKT-PH-mCherry was as expected, more uniformly distributed (Fig. 6C). Quantitatively, it was evident from the signal intensity plots (see methods) in figure 6D, that a gradient of PIP3 is established during phagocytosis, with the highest concenration at the site of entry. Moreover since blocking the entry of extracellular Ca^{2+} either through chelators or inhibitors of voltage gated channels resulted in a loss of PIP3 gradient in a similar fashion as in the case of wortmannin treatment, it was evident that the formation of PIP3 gradient was dependent on Ca^{2+}, more liekly on the entry of Ca^{2+} from extracellular milieu through the voltage-gated Ca^{2+} channels (Fig. 6D). Together these results imply that the extracellular Ca^{2+}, entering through a voltage-gated Ca^{2+} channel helps forming the foci for the recruitment of PI3K and initiate the signaling cascade for phagocytic uptake in the macrophages.

Mannosidase-II positive early phagosomes are also NCS1 positive

Having established the role of Ca^{2+} in regulating the movement of Mannosidase-II vesicles during phagocytosis, we next wanted to understand how the focal movement of Golgi-derived vesicles is triggered in phagocytosing macrophages. NCS1 is an EF-hand motif containing protein, originally believed to exclusively express in the neuronal cells (Haynes et al., 2005). Subsequently it was shown to get expressed in a variety of cell lines as TGN resident Ca^{2+} interacting protein (Haynes et al., 2005). NCS1 was reported to be involved in the recruitment of Golgi-derived vesicles during plasma membrane repair in macrophages and was integral to these vesicles (Behar et al., 2010; Divangahi et al., 2009). In cells expressing mCherry-MAN2A we stained for NCS1 during uptake of latex beads or Mtb. In both the cases, NCS1 co-localized

with the cargo (Fig. 7A, Fig. S7A). In the case of Mtb, nearly all Mtb containing phagosomes were also positive for NCS1 whereas some NCS1 positive phagosomes did not contain Mannosidase-II (Fig. 7A). Similarly for beads, NCS1 intensity was much higher compared to Mannosidase-II intensity (Fig. 7B). Moreover, we observed NCS1 to co-localize with Mannosidase-II in vesicles that were not part of the phagosome (Fig. S7B), corroborating with the fact that both Mannosidase-II and NCS1 are components of the GA secretory vesicles derived from the GA (Behar et al., 2010; Divangahi et al., 2009).

Depleting Neuronal Calcium Sensor 1 (NCS1) inhibits focal exocytosis of MAN2A vesicle during phagocytosis

To test whether Ca^{2+} dependent trigger of vesicular trafficking relied on the ability of NCS1 activation upon Ca^{2+} binding, we compared the recruitment of Mannosidase-II at the nascent phagosome during phagocytosis of *E. coli* in THP-1 macrophages that were either treated with scrambled siRNA control or NCS1 specific siRNA (Fig. S7C). Knocking down NCS1 resulted in more than 50% decline in the recruitment of Mannosidase-II at the early *E. coli* phagosomes (Fig. 7C). Expectedly, knockdown of NCS1 in THP-1 macrophages resulted in a marked decline in the uptake of latex beads, *E. coli*, *Salmonella* and *Mtb* (Fig. 7D). True to all other treatments, which inhibited the phagocytic uptake, NCS1 siRNA knockdown also had both quantitative and kinetic effects on the uptake of all of the targets except in *Salmonella* where the effects were persistent (Fig. 7D). Thus uptake in case of latex beads was ~35, 60 and 85% of the control in the siRNA treated sets at 30 minutes, 1 hours and 2 hours respectively (Fig. 7D). For *E. coli* these numbers were 8, 10 and 22% of control at 5, 15 and 30 minutes (Fig. 7D). In case of *Salmonella*, uptake was about 65% of the control set at 15 and 30 minutes while in case of *Mtb*, the relative uptake in the NCS

420 knockdown cells was 40, 45 and 55% of control at 1 hour, 2 hours and 4 hours
421 respectively (Fig. 7D).
422

Discussions

Professional phagocytes like macrophages require continuous supply of membrane in order to form phagosomes around the phagocytosed particles (Vicker, 1977). It is now understood that cellular compartments like recycling endosomes, lysosomes and ER could supply membrane for the nascent phagosomes (Bajno et al., 2000; Tardieux et al., 1992)' (Gagnon et al., 2002). Adding to the existing pool of membrane sources available for phagosome formation, in this study we show recruitment of Golgi-derived vesicles at the site of phagocytosis in macrophages. However unlike previous reports, where the studies were mostly restricted to either latex beads or select organism, we show here a more universal requirement of the Golgi-derived vesicles during phagocytosis by macrophages using inert particles, non-pathogenic bacteria and two different pathogenic bacterial species as the cargo. It is important to note here that GA serves as the origin for most vesicles in the cell, including recycling endosomes, endocytic machinery and vesicles destined to the plasma membrane for exocytosis (Bonifacino and Glick, 2004). Bacterial pathogens once inside the host cells further subvert the membrane trafficking pathways to ensure prolonged survival and escape from innate defense mechanisms(Alix et al., 2011). Interestingly GA serves as the hub for trafficking inside the cells (Gillingham and Munro, 2016). It therefore may make strong sense that GA gets involved and alerted of incoming pathogen while the cell has just started to engulf it. This line of investigation seems extremely fascinating at present as it may open a new understanding in the functioning of innate immune system.

Role of Golgi-derived vesicles in supplying the membrane at plasma membrane is well known at least in one context - the membrane repair pathway (Divangahi et al., 2009). Using Mannosidase-II as specific marker for Golgi-derived vesicles they

showed participation of GA and lysosomes in the repair process through targeted exocytosis (Divangahi et al., 2009). The movement of vesicles during phagocytosis from the recycling endosomes and lysosomes was also reported to follow a similar targeted exocytosis where vesicles are directed towards the phagocytic cup (Bajno et al., 2000; Niedergang and Chavrier, 2004; Samie et al., 2013). Interestingly more than 90% of Mannosidase-II positive phagosomes at the site of entry were also found to be positive for VAMP-3 and dynamin-2. While VAMP-3 gets recruited through focal exocytosis, dynamin-2 is known to regulate post-Golgi transport of vesicles and facilitate focal exocytosis (Samie et al., 2013). Dynamins have earlier been implicated in regulating the focal exocytosis in phagocytosing macrophages (Di et al., 2003; Gold et al., 1999; Samie et al., 2013). Inhibition of dynamins by dynasore treatment resulted in a reduced phagocytic uptake, which may simply occur due to inhibition of dynamin-mediated scission of phagosomes from the membrane (Jones et al., 1998). However dynasore treatment also resulted in reduced Mannosidase-II recruitment at the nascent phagosomes, implying the involvement of roles dynamin plays in vesicle budding and their focal movement towards the site of uptake. High co-localization of Mannosidase-II with TfR further emphasized very early recruitment of Golgi-derived vesicles. Yet another instance where vesicle exocytosis from Golgi has been extensively studied is in the context of neurotransmitter release, which shows remarkable similarity with the focal exocytosis during membrane repair. Thus it is intriguing to witness the brilliance of cellular economy, where a common mechanism could be utilized to address three entirely independent cellular requirements.

Next to understand how target recognition at the cell surface for phagocytic uptake could trigger GA to elicit the movement of the vesicles, we took cues from membrane repair pathway where the damage is typically sensed via entry of extracellular Ca^{2+}

into the cells (Miyake and McNeil, 1995; Steinhardt et al., 1994). We indeed observed inhibiting either extracellular Ca^{2+} or the release of Ca^{2+} from intracellular stores resulted in a loss of phagocytic function in the macrophages. The possibility of a membrane breach during phagocytic uptake in macrophages has never been discussed. Thus most plausible source for the entry of extracellular Ca^{2+} was some membrane channels, which are classically involved at a similar step during neurotransmitter release(Augustine, 2001; Sudhof, 2012). Experiments with loperamide and amlodipine strongly support a critical involvement of voltage-gated Ca^{2+} channel in the extracellular Ca^{2+} entry thereby facilitating phagocytosis. Incidentally the role of voltage-gated channel in regulating podosome formation in the macrophages was recently shown (Carrithers et al., 2009). Yet another channel TRPV2 was recently shown to be important for phagocytosis in macrophages and its absence resulted in loss of Ca^{2+} influx from the extracellular milieu and abrogated phagocytic uptake (Link et al., 2010). Curiously macrophages lacking TRPV2 were also defective in chemoattractant-evoked motility (Link et al., 2010). It may not be unusual to assume that some of the inhibitory effects shown in this study were most likely due to inhibition of TRPV channels at the plasma membrane. Therefore it seems macrophage membrane depolarization could be a more general mechanism of cellular functioning including phagocytosis, adherence and motility.

Phagocytosis was also dependent on the release of Ca^{2+} from intracellular stores, as TMB8 treatment inhibited phagocytosis. A combination of EGTA and TMB8 had more dramatic effects on phagocytosis, which also showed some sort of selectivity in terms of the cargo. Thus, for latex beads, blocking both intra- and extra-cellular cargo abolished their uptake by the macrophages, however in case of bacteria, the block in uptake was more kinetic in nature. It strongly supports the possibility that Ca^{2+} may

be extremely critical for the uptake of cargos where cognate receptors are not known/available thereby rely a lot on the membrane depolarization and associated Ca^{2+} entry. The graded importance of Ca^{2+} during phagocytosis of diverse targets needs further exploration for better understanding. Inhibition of Ca^{2+} also resulted in reduced Mannosidase-II recruitment at the phagosomes.

The role of PI3Kinase in phagocytosis is well known, which supposedly helps pseudopod extension while engulfing the target (Cox et al., 1999). However, it has also been shown that inhibition of PI3Kinase may limit the membrane availability (Underhill and Ozinsky, 2002). We indeed observed uptake of *Mtb*, *Salmonella* or latex beads by macrophages were severely compromised in the presence of wortmannin. *Salmonella* entry is known to occur via either macropinocytosis or phagocytosis, however the former is insensitive to PI3Kinase inhibition(Drecktrah et al., 2006). Thus the strains used in this study taken up by the macrophages thorugh phagocytosis. Interestingly vesicle recruitment has also been reported to be important for membrane ruffle formation, which helps in Salmonella macropinocytosis (Dai et al., 2007). We also noted significantly reduced recruitment of Mannosidase-II vesicles at the nascent phagosomes in the presence of wortmannin. Thus recruitment of Golgi-derived vesicles at the nascent phagosomes indeed required PIP3. Experiments with AKT-PH-mCherry clearly support the establishment of PIP3 gradient during phagocytosis. Selective PIP3 enrichment has previously been shown regulating cellular polarity, chemotaxis and pseudopod extension (Cox et al., 1999; Funamoto et al., 2002; Ridley et al., 2003). The most dramatic observation was however the use of voltage-gated Ca^{2+} channels by macrophages to set the foci for PIP3 accumulation, which eventually results in all the downstream signaling and recruitments. Interestingly, dynamins have conserved PH-domain at their C-terminal, making them

523 responsive to the PIP3 levels. It has been shown that mutations in the PH domain of
524 dynamin could result in severe defects in its key functioning like post-Golgi transport
525 and endocytosis (Achiriloaie et al., 1999; Zuchner et al., 2005). Thus PI3K and
526 dynamins seem to work together for the focal recruitment of Golgi-derived vesicles
527 during phagosome biogenesis.
528 The Ca^{2+} sensing function in the GA is attributed to the resident molecule NCS1,
529 which was initially discovered in the neuronal cells regulating the synaptic
530 transmission (Haynes et al., 2005). NCS1 was also shown as part of the secretory
531 vesicles (Scalettar et al., 2002). In macrophages, ablation of NCS1 resulted in a block
532 in the membrane-resealing pathway (Divangahi et al., 2009). We therefore
533 hypothesized; NCS1 could also serve as the Ca^{2+} sensor in Golgi apparatus for
534 triggering the exodus of the vesicles during phagocytosis. Interestingly, NCS1
535 knockdown not only reduced the phagocytic function of macrophages, there was also
536 significantly lower recruitment of Mannosidase-II at the phagosomes.
537 The results form purified latex beads phagosomes supported the overall observation in
538 this study that phagocytic uptake is a complex process and involves several players.
539 We deliberately focused on the molecules below 25kDa cut-off to make sure
540 enrichment of three key classes of molecules including RABs (~25 kDa), ARFs (~20
541 kDa) and VAMPs (~14 kDa). This was to ensure that the presence of other high
542 abundance and high molecular weight proteins did not mask these low abundant low
543 molecular weight proteins. We identified 17 different RABs on the phagosomes out of
544 which nine were associated with Golgi function. We also identified five out of six
545 known ARFs, where ARF1 and ARF3 were particularly important for their known
546 association with Golgi apparatus, phagosome/engulfment and exocytosis(Beck et al.,
547 2008; Faundez et al., 1997; Krauss et al., 2008). We could identify four different

548 VAMPs in the phagosomes including VAMP2, 3, 4 and 8. While role of VAMP3 in
549 phagosome biogenesis is well described, VAMP2 is particularly known for its
550 involvement in exocytosis, neurotransmitter release and secretory vesicles (Faurschou
551 and Borregaard, 2003; Shen et al., 2015). Previously in a proteomic study of the latex-
552 beads containing phagosome, VAMP4 was identified as phagosome membrane
553 associated protein (Shui et al., 2008). VAMP4 are trans-Golgi resident proteins and
554 are also involved in the immature secretory granules (Steegmaier et al., 1999). We
555 also found SEC22B in the phagosome MS data, an important SNARE known to be
556 important for the recruitment of ER during phagocytic uptake (Becker et al., 2005).
557 Considering the number of RABs, ARFs and VAMPs associated with the exocytosis
558 and secretory vesicles, it seems very likely that the true identity of the Golgi-derived
559 vesicles that are recruited during phagosome biogenesis could be secretory vesicles.
560 However the role of GA during phagocytosis was ruled out in the past since
561 phagocytic uptake was found insensitive to Brefeldin A (Becker et al., 2005), a fungal
562 metabolite, which disrupts the GA (Lippincott-Schwartz et al., 1989). Interestingly
563 during membrane repair process, which is also dependent on secretory vesicles from
564 GA in addition to other membrane sources, while the repair of first wound is typically
565 independent of Brefeldin A, it has been reported that repair of any subsequent wounds
566 are sensitive to Brefeldin A (Andrews, 2002; Togo et al., 2000). Similarly during
567 secretion, Brefeldin A while inhibits the formation of new secretory vesicles, does not
568 interfere with the membrane fusion of pre-formed vesicles (Miller et al., 1992; Rosa
569 et al., 1992). Thus it is possible that following exhaustion of pre-formed vesicles
570 during phagocytosis, uptake of any subsequent cargo encountered by the cell may
571 show sensitivity to BFA. This is an interesting proposition and certainly warrants
572 further investigations.

573 At the molecular level it seems SNARE mediated fusion may be involved in the
574 phagosome biogenesis. We were able to track the presence of syntaxin 1, the t-
575 SNARE at the plasma membrane involved in SNARE mediated vesicle fusion, along
576 with Mannosidase-II at the early phagosomes (Fig S7D). Syntaxin-1 is known to
577 facilitate fusion of secretory vesicles(Sollner et al., 1993). Moreover, its presence will
578 also be required for the fusion of VAMP3 positive vesicles, a vSNARE typically
579 located in the recycling endosomes. Given the multiplicity of v-SNAREs and t-
580 SNAREs with possibly overlapping functions makes it challenging to clearly establish
581 the fusion machinery involved. The identity of SNAREs involved in this process
582 therefore constitutes the next set of challenge following this study. Taken together the
583 results in this study allowed us to reconstruct the process of phagocytosis (Fig. 7E).
584 We note that Golgi-derived vesicles are one of the several sub-cellular vesicular pools
585 available for phagosome biogenesis including recycling endosomes and lysosomes. It
586 actually explains why in many cases except for PI3K inhibition, the effects were more
587 kinetic in nature. We did observe in our results cases where some phagosomes were
588 only positive for VAMP3 and not Mannosidase-II or vice-versa, leaving us with an
589 intriguing question that whether the outcome of phagocytosis could vary depending
590 on which organelle contributed the most for the formation of phagosome.
591 In conclusion, we show here an as yet unknown function of Golgi-derived vesicles
592 during phagocytic uptake in macrophages. The targeted exocytosis coupled with
593 phagocytosis has been studied in the past, however involvement of vesicles from the
594 GA in macrophages is unprecedented. Similarly regulation of phagocytic uptake by
595 NCS1 comprehensively extends the known functions of this molecule in
596 macrophages. Finally our finding that the voltage-gated Ca^{2+} channel could play a
597 role in the process of phagocytosis may be potentially harnessed in future for

598 developing better therapeutic interventions for various infectious diseases including
599 tuberculosis.
600

601 # Methods

602 ## Ethics statement

603 The animal experiments were performed upon prior approval from the institutional
604 ethics committee (IAEC) of International Center for Genetic Engineering and
605 Biotechnology (Approval no.: ICGEB/AH/2013/03/IMM-38).

606 **Reagents And Antibodies:** The following reagents were used in this study:
607 Wortmannin (Sigma Aldrich,W1628), Dynasore Hydrate (Sigma Aldrich, D7693),
608 Nocodazole (Sigma Aldrich, M1404), TMB8 (Sigma Aldrich, T111), EGTA
609 (Amresco, 0732), Loperamide (Sigma Aldrich, L4762), Amlodipine besylate (Sigma
610 Aldrich, A5605), PKH 67 (Sigma Aldrich, MINI 26), RIPA buffer (Amresco,N653),
611 BSA (Sigma Aldrich, A2153), Saponin (Sigma Aldrich, 47036), Puromycin
612 (Invivogen, ant-pr-1), 4 µm aldehydate-sulphatelatex beads (Life Technologies,
613 A37304) and 1µm yellow green aldehyde latex beads (Life Technologies, F8823).
614 All the siRNA used in this study were siGenome siRNA SmartPool (Dharmacon Inc).
615 The transfection reagent used for siRNA transfections was Dharmafect-2 (Dharmacon
616 Inc). The primary antibodies used in this study are: Mannosidase II (abcam, ab12277),
617 Dynamin (Santacruz, sc-6401), VAMP3 (abcam, ab43080), Transferrin (abcam,
618 ab84036). The secondary antibodies used in this study are: Alexa fluor 405 and Alexa
619 fluor 568 conjugates from (Life Technologies). **Plasmid Constructs:** The plasmid
620 constructs used in this study are mCherry-ManII-N-10 (Addgene plasmid #55073),
621 pcDNA3.1_AktPH-mCherry (Addgene plasmid #67301), pCT- Golgi-GFP
622 (CYTO104-VA-1) and pCT-Mem-GFP (System Biosciences, CYTO100-PA-1).

623 **Bacterial Culture Maintainence:** Mycobacterial cultures were maintained in 7H9
624 media (Difco) supplemented with 10% OADC. Single cell suspension of
625 Mycobacterial strains were prepared by aspiration of the culture eight times with 26
626 gauge needle and six times 30 gauge needles. Quantification of this prepared culture
627 was done by taking absorbance at 600 nm wavelength (0.6 O.D. corresponds to ~100
628 x 10^6 bacteria). The bacteria thus appropriately calculated were added to the cells at
629 the mentioned MOI (Multiplicity of Infection). For microscopy experiments, the
630 desired number of bacteria was stained with PKH67 (Sigma Aldrich), a lipophilic
631 green fluorescent dye, as per the manufacturer's protocol. The stained bacteria were
632 then passed thrice through a 26-gauge needle and used for infection. *E. coli* and
633 *Salmonella* Typhimurium strains were maintained in LB (Difco). For infection culture
634 density was determined by OD at 600 for both *E. coli* and *S.*Typhimurium containing
635 GFP, an OD of 1= 1 x 10^8 bacteria for both these strains.
636 **Tissue Culture:** THP-1 cells (a kind gift from Dr. Dong An, UCLA) and U937 cells
637 (ATCC) were cultured in RPMI 1640 medium (Life Technologies) and RAW264.7
638 (ATCC) murine macrophages were grown in Dulbecco's modified Eagle's media
639 (DMEM, Life Technologies) supplemented with 10% Fetal Bovine Serum (FBS,
640 GIBCO) and maintained 37^{o}C in a humidified, 5% CO_2 atmosphere. THP1 cells were
641 differentiated with 20ng/µl PMA for 24 hours, washed with plain RPMI and
642 maintained in 10% FCS supplemented RPMI for another 24 hours. The cells were
643 then infected with respective bacteria/beads. RAW264.7 macrophages were seeded in
644 respective plates and differentiated with 200ng/ml LPS for 12 hours. The cells were
645 washed once with plain DMEM and infected with respective bacteria/beads.
646 **Animals and isolation of BMDMs**

Bone marrow derived macrophages (BMDMs) were isolated from femurs of BALB/C mice (4-6 weeks old, female) obtained from institutional animal house. BMDMs were obtained by culturing the marrow cells in the presence of macrophage-colony stimulating factor (M-CSF, eBioscience, 14-8983-80) for 7 days. Fully differentiated macrophages were harvested and seeded for infection with H37Rv. The infection protocol was same as described above for THP-1 macrophages.

Experiments with Latex beads: For microscopy experiments 4µm aldehyde sulfate latex beads (Life Technologies) were incubated with human/mouse IgG on an agitator overnight. The beads were washed twice with plain DMEM by centrifugation at 2000 rpm for 10 minutes and added to cells at respective MOI. For flow cytometry experiments, 1µm FITC labeled aldehyde beads were added at respective MOI to the differentiated THP1 cells.

Transfection & Nucleofection Assays: Transfection & Transduction was carried out using JetPrime Reagent (Himedia) as per the manufacturer's protocol. Nucleofection was carried out with the 4D-Nucleofector™ System Lonza in 20 µl Nucleocuvette™ Strips with program DS-136, as per the manufacturer's protocol. At 24 hours post Nucleofection these cells expressed the inserted vector as determined by visualization with a fluorescence microscope.

siRNA Transfection & Inhibitor Assays: Post 24 hours of PMA treatment, the cells were washed once with plain RPMI. The siRNA's were added as per the manufacturer's protocol. Post 48 hours of incubation the respective infection/assays were performed. For the inhibitor assays such as, Dynasore(40µM, 80µM), Wortmannin (as specified) were added 4 hours before infection. While Nocodazole(25 µM) was added 2.5 hours before infection and EGTA(3mM),

672 TMB8(100 μM), Loperamide hydrochloride(100 μM) and Amlodipine besylate(100
673 μM) were added for 30 minutes before infection.

674 **Creation of stable cell lines:** The stable cell lines were created from lentivirus
675 cytotracer plasmids (B4GALT1-mRuby and NEUM-EGFP, System Biosciences).
676 $1X10^6$ U937 cells were added to a 24 well plate. The harvested media containing
677 lentivirus (refer to transfection section) was added to them. At 72 hours post infection
678 the cells were selected on Puromycin at 350ng/ml for 21 days. The population of
679 positive cells was routinely checked by microscopy and it was found that post
680 selection for 21 days the population of cells remained stable (in our case 30-40%).

681 **Staining for Confocal Microscopy:** At specific time points cells were fixed with 4%
682 Paraformaldehyde (PFA) for 15 minutes. This was followed by 2 washes with 1x
683 PBS. The cells were permeabilized with 0.4% Triton X- 100 for 30 minutes and
684 washed once with 1X PBS. Blocking was performed using 3 %(w/v) BSA and
685 0.5%Tween-20 in 1X PBS for one hour, followed by one wash with 1X PBS. The
686 cells were now stained with respective primary antibody made in the blocking
687 solution at specific dilution for 90 minutes. The coverslips were then washed once
688 with 1X PBST and twice with 1X PBS. This was followed by staining with respective
689 secondary antibody tagged with fluorophore of choice for 90 minutes. The primary
690 and secondary antibodies were diluted in blocking solutions for use. After three
691 washes with 1X PBS, the coverslips were then mounted on glass slides with anti-fade
692 reagent(Life Technologies). Images were acquired with Nikon A1R Laser Scanning
693 Confocal Microscope with a 100X/1.4NA Plan Apochromat VC, DIC N2 objective
694 lens. Image processing viz. 3D reconstruction, co-localization and intensity
695 measurements were done via Imaris 7.2 (Bitplane).

Live Cell Imaging: The live cell imaging dish pre-seeded was RAW264.7 macrophages expressing mCherry-MAN2A. The live cell system was set at 5% CO_2 and 37^0C. The field was set and imaged for 10 minutes. This was followed by an on-stage addition of 0.0001% saponin for 5 minutes. The cells were washed once, supplemented with complete media and imagining continued. The entire procedure was performed on stage to analyze the pre- and post treatment effects on the membrane under our experimental set up.

Flow Cytometry experiments: At respective time points, the infected cells were washed thrice with sterile 1X PBS to remove extracellular bacteria/beads and fixed with 2% PFA. The cells were scraped and run on BD FACS Canto or BD FACS Influx cytometer's.

Western Blot: Post SDS PAGE, the proteins were blotted onto a nitrocellulose membrane using a semidry-transfer system. Following incubation with primary and secondary antibodies, the blots were scanned using Odyssey InfraRed Imaging System (LI-COR BioSciences, Lincoln, NE, USA) at various intensities in order to obtain a blot scan with minimum background. All settings were rigorously maintained for all experiments. The scans were quantitatively analyzed using Odyssey InfraRed Imaging System Application Software_Version.3.O (commercially available from (LI-COR BioSciences, Lincoln, NE, USA).

Phagosome Isolation: Latex bead phagosome for 1µm latex beads were isolated as per protocol described earlier (Desjardins et al., 1994). At 1 hour post addition, the plates were washed 4 times with cold 1XPBS, ensuring all the extracellular beads were completely washed off. The cells were scraped off with a rubber policeman and centrifuged twice with cold 1XPBS at 1200 RPM for 5 minutes. The cells were pooled and washed once with homogenization buffer at 1200 RPM for 5 Minutes

(3mM imidazole, 250 mM sucrose, pH 7.4). The cells were then incubated in appropriate volume of homogenization buffer (with protease inhibitor cocktail – Amresco) for 30 minutes. The cells were lysed by dounce homogenizer till 90% of the cells were disrupted as observed under a light microscope. This lysate was centrifuged at 1200 RPM for 5 minutes at 4^0C to remove the unbroken cells. This was followed by preparation of sucrose gradient for ultracentrifugation. The homogenate was made to be consisting of 40% sucrose by mixing with equal volume of 62% sucrose and 2.25 ml of the same was layered upon 2.0ml of 62% sucrose solution. We then added 2.25 ml each of 35%, 25% and 10% sucrose solutions. The tubes were centrifuged at 100,000g for 1 hour at 4^0C in an SW28 rotor (Beckman Coulter). The LBC band obtained between 10 and 25% sucrose layers was collected and washed once with cold 1XPBS at 40,000g at 4^0C in an SW28 rotor (Beckman Coulter).

Mass Spectrometry & Data Analysis: For LC-LTQ Orbitrap MS analysis, samples were re-solubilized in 2% [v/v] acetonitrile, 0.1% [v/v] formic acid in water and injected onto the trap column at a flow rate of 20 µl/min subsequently peptides were separated on Zorbax 300SB-C18 (Agilent, Santa Clara, CA, USA) by a gradient developed from 2% [v/v] acetonitrile, 0.1% [v/v] formic acid to 80% [v/v] acetonitrile, 0.1% [v/v] formic acid in water over 180 min at a flow rate of 300 nl/min onto an Agilent 1200 (Agilent, Santa Clara, CA, USA) nano-flow LC-System that was in-line coupled to the nano-electrospray source of a LTQ-Orbitrap discovery hybrid mass spectrometer (Thermo Scientific, San Jose, CA, USA). Full MS in a mass range between m/z 300-2,000 was performed in the Orbitrap mass analyzer with a resolution of 30,000 at m/z 400 and an AGC target of 2x 105. The strongest five signals were selected for CID (collision induced dissociation)-MS/MS in the LTQ ion trap at a normalized collision energy of 35% using an AGC target of 1x 105 and two

746 microscans. Dynamic exclusion was enabled with one repeat counts during 45 s and
747 an exclusion period of 180 s. Peptide identification was performed by CID-based
748 MS/MS of the selected precursors. For protein/peptide identification, MS/MS data
749 were searched against the *Mus musculus* amino acid sequence database (downloaded
750 in August 2015) using an in-house Mascot server (version 2.4) through the Proteome
751 Discoverer 1.4 software. The search was set up for full tryptic peptides with a
752 maximum of three missed cleavage sites- carbamidomethyl on cysteine, and oxidized
753 methionine were included as variable modifications. The precursor mass tolerance
754 threshold was 10 ppm, and the maximum fragment mass error was 0.8 Da. The
755 significance threshold of the ion score was calculated based on a false discovery rate
756 of <1%, estimated by the peptide validator node of the Proteome Discoverer software.
757 **Analysis for functional classes:**
758 The non-redundant list of proteins identified was matched against a series of gene
759 ontology classes from AMIGO2 database. The selection of gene ontology was
760 empirically made based on known and perceived classes, which together could
761 represent the set of trafficking proteins identified. The obtained matches were then
762 represented as a network using Cytoscape 3.2.0.
763 **Statistical Analysis:**
764 Comparative groups were analyzed using paired two-tailed t-test using inbuilt
765 function in MS Excel.
766 **3-D recreation and analysis:** The intensity of a particular fluorophore on the bead
767 was estimated by first creating a three dimensional bead surface in the captured image
768 (z-stack) using “spot module” in Imaris Version 7.2 (Bitplane) which automatically
769 detects spheres in an image depending upon the dimensions fed. The software then
770 allows one to determine fluorescence intensity on the surface individually for each

fluorophore. For each case maximum fluorescence intensity was determined and plotted.

PIP3 gradient analysis: The gradient of fluorescence in the AKT-pH mCherry experiments was determined using "intensity profile line tool" in NIS-Elements (NIKON).

ACKNOWLEDGEMENTS

The work was supported by a grant from the Department of Biotechnology (DBT), Govt. of India (BT/PR14730/BRB/10/874/2010, DK) and partly by International AIDS Society and CFAR funded CNIHR grant from NIH, USA (DK). The work related to *Mycobacterium tuberculosis* infections were carried out at DBT funded TACF facility at ICGEB. We thank Prof. Sarman Singh for access to the flow-cytometer at AIIMS and Purnima for her help in the confocal microscopy. We thank C-CAMP, NCBS, Bangalore for the mass spectrometry facility. NV is a recipient of a senior research fellowship from the University Grants Commission, India.

References

Achiriloaie, M., B. Barylko, and J.P. Albanesi. 1999. Essential role of the dynamin pleckstrin homology domain in receptor-mediated endocytosis. *Molecular and cellular biology*. 19:1410-1415.

Aderem, A., and D.M. Underhill. 1999. Mechanisms of phagocytosis in macrophages. *Annual review of immunology*. 17:593-623.

Alix, E., S. Mukherjee, and C.R. Roy. 2011. Subversion of membrane transport pathways by vacuolar pathogens. *The Journal of cell biology*. 195:943-952.

Andrews, N.W. 2002. Lysosomes and the plasma membrane: trypanosomes reveal a secret relationship. *The Journal of cell biology*. 158:389-394.

Augustine, G.J. 2001. How does calcium trigger neurotransmitter release? *Current opinion in neurobiology*. 11:320-326.

Bainton, D.F., R. Takemura, P.E. Stenberg, and Z. Werb. 1989. Rapid fragmentation and reorganization of Golgi membranes during frustrated phagocytosis of immobile immune complexes by macrophages. *The American journal of pathology*. 134:15-26.

Bajno, L., X.R. Peng, A.D. Schreiber, H.P. Moore, W.S. Trimble, and S. Grinstein. 2000. Focal exocytosis of VAMP3-containing vesicles at sites of phagosome formation. *The Journal of cell biology*. 149:697-706.

Beck, R., Z. Sun, F. Adolf, C. Rutz, J. Bassler, K. Wild, I. Sinning, E. Hurt, B. Brugger, J. Bethune, and F. Wieland. 2008. Membrane curvature induced by Arf1-

GTP is essential for vesicle formation. *Proceedings of the National Academy of Sciences of the United States of America*. 105:11731-11736.

Becker, T., A. Volchuk, and J.E. Rothman. 2005. Differential use of endoplasmic reticulum membrane for phagocytosis in J774 macrophages. *Proceedings of the National Academy of Sciences of the United States of America*. 102:4022-4026.

Beemiller, P., A.D. Hoppe, and J.A. Swanson. 2006. A phosphatidylinositol-3-kinase-dependent signal transition regulates ARF1 and ARF6 during Fcgamma receptor-mediated phagocytosis. *PLoS biology*. 4:e162.

Behar, S.M., M. Divangahi, and H.G. Remold. 2010. Evasion of innate immunity by Mycobacterium tuberculosis: is death an exit strategy? *Nature reviews. Microbiology*. 8:668-674.

Bonifacino, J.S., and B.S. Glick. 2004. The mechanisms of vesicle budding and fusion. *Cell*. 116:153-166.

Braun, V., C. Deschamps, G. Raposo, P. Benaroch, A. Benmerah, P. Chavrier, and F. Niedergang. 2007. AP-1 and ARF1 control endosomal dynamics at sites of FcR mediated phagocytosis. *Molecular biology of the cell*. 18:4921-4931.

Braun, V., and F. Niedergang. 2006. Linking exocytosis and endocytosis during phagocytosis. *Biology of the cell / under the auspices of the European Cell Biology Organization*. 98:195-201.

Cannon, G.J., and J.A. Swanson. 1992. The macrophage capacity for phagocytosis. *Journal of cell science*. 101 (Pt 4):907-913.

Carrithers, M.D., G. Chatterjee, L.M. Carrithers, R. Offoha, U. Iheagwara, C. Rahner, M. Graham, and S.G. Waxman. 2009. Regulation of podosome formation in macrophages by a splice variant of the sodium channel SCN8A. *The Journal of biological chemistry*. 284:8114-8126.

Chen, Y.A., and R.H. Scheller. 2001. SNARE-mediated membrane fusion. *Nature reviews. Molecular cell biology*. 2:98-106.

Church, J., E.J. Fletcher, K. Abdel-Hamid, and J.F. MacDonald. 1994. Loperamide blocks high-voltage-activated calcium channels and N-methyl-D-aspartate-evoked responses in rat and mouse cultured hippocampal pyramidal neurons. *Molecular pharmacology*. 45:747-757.

Cox, D., C.C. Tseng, G. Bjekic, and S. Greenberg. 1999. A requirement for phosphatidylinositol 3-kinase in pseudopod extension. *The Journal of biological chemistry*. 274:1240-1247.

Czibener, C., N.M. Sherer, S.M. Becker, M. Pypaert, E. Hui, E.R. Chapman, W. Mothes, and N.W. Andrews. 2006. Ca2+ and synaptotagmin VII-dependent delivery of lysosomal membrane to nascent phagosomes. *The Journal of cell biology*. 174:997-1007.

Dai, S., Y. Zhang, T. Weimbs, M.B. Yaffe, and D. Zhou. 2007. Bacteria-generated PtdIns(3)P recruits VAMP8 to facilitate phagocytosis. *Traffic*. 8:1365-1374.

Desjardins, M., L.A. Huber, R.G. Parton, and G. Griffiths. 1994. Biogenesis of phagolysosomes proceeds through a sequential series of interactions with the endocytic apparatus. *The Journal of cell biology*. 124:677-688.

Di, A., D.J. Nelson, V. Bindokas, M.E. Brown, F. Libunao, and H.C. Palfrey. 2003. Dynamin regulates focal exocytosis in phagocytosing macrophages. *Molecular biology of the cell*. 14:2016-2028.

855 Divangahi, M., M. Chen, H. Gan, D. Desjardins, T.T. Hickman, D.M. Lee, S. Fortune,
856 S.M. Behar, and H.G. Remold. 2009. Mycobacterium tuberculosis evades
857 macrophage defenses by inhibiting plasma membrane repair. *Nature*
858 *immunology*. 10:899-906.
859 Drecktrah, D., L.A. Knodler, R. Ireland, and O. Steele-Mortimer. 2006. The
860 mechanism of Salmonella entry determines the vacuolar environment and
861 intracellular gene expression. *Traffic*. 7:39-51.
862 Faundez, V., J.T. Horng, and R.B. Kelly. 1997. ADP ribosylation factor 1 is required
863 for synaptic vesicle budding in PC12 cells. *The Journal of cell biology*.
864 138:505-515.
865 Faurschou, M., and N. Borregaard. 2003. Neutrophil granules and secretory
866 vesicles in inflammation. *Microbes and infection / Institut Pasteur*. 5:1317-
867 1327.
868 Flannagan, R.S., V. Jaumouille, and S. Grinstein. 2012. The cell biology of
869 phagocytosis. *Annual review of pathology*. 7:61-98.
870 Funamoto, S., R. Meili, S. Lee, L. Parry, and R.A. Firtel. 2002. Spatial and temporal
871 regulation of 3-phosphoinositides by PI 3-kinase and PTEN mediates
872 chemotaxis. *Cell*. 109:611-623.
873 Gagnon, E., S. Duclos, C. Rondeau, E. Chevet, P.H. Cameron, O. Steele-Mortimer, J.
874 Paiement, J.J. Bergeron, and M. Desjardins. 2002. Endoplasmic reticulum-
875 mediated phagocytosis is a mechanism of entry into macrophages. *Cell*.
876 110:119-131.
877 Gillingham, A.K., and S. Munro. 2007. The small G proteins of the Arf family and
878 their regulators. *Annual review of cell and developmental biology*. 23:579-
879 611.
880 Gillingham, A.K., and S. Munro. 2016. Finding the Golgi: Golgin Coiled-Coil
881 Proteins Show the Way. *Trends in cell biology*.
882 Gold, E.S., D.M. Underhill, N.S. Morrissette, J. Guo, M.A. McNiven, and A. Aderem.
883 1999. Dynamin 2 is required for phagocytosis in macrophages. *The*
884 *Journal of experimental medicine*. 190:1849-1856.
885 Haynes, L.P., G.M. Thomas, and R.D. Burgoyne. 2005. Interaction of neuronal
886 calcium sensor-1 and ADP-ribosylation factor 1 allows bidirectional
887 control of phosphatidylinositol 4-kinase beta and trans-Golgi network-
888 plasma membrane traffic. *The Journal of biological chemistry*. 280:6047-
889 6054.
890 Henley, J.R., and M.A. McNiven. 1996. Association of a dynamin-like protein with
891 the Golgi apparatus in mammalian cells. *The Journal of cell biology*.
892 133:761-775.
893 Holevinsky, K.O., and D.J. Nelson. 1998. Membrane capacitance changes
894 associated with particle uptake during phagocytosis in macrophages.
895 *Biophysical journal*. 75:2577-2586.
896 Jones, S.M., K.E. Howell, J.R. Henley, H. Cao, and M.A. McNiven. 1998. Role of
897 dynamin in the formation of transport vesicles from the trans-Golgi
898 network. *Science*. 279:573-577.
899 Jutras, I., and M. Desjardins. 2005. Phagocytosis: at the crossroads of innate and
900 adaptive immunity. *Annual review of cell and developmental biology*.
901 21:511-527.
902 Kochegarov, A.A. 2003. Pharmacological modulators of voltage-gated calcium
903 channels and their therapeutical application. *Cell calcium*. 33:145-162.

Koul, A., T. Herget, B. Klebl, and A. Ullrich. 2004. Interplay between mycobacteria and host signalling pathways. *Nature reviews. Microbiology*. 2:189-202.

Krauss, M., J.Y. Jia, A. Roux, R. Beck, F.T. Wieland, P. De Camilli, and V. Haucke. 2008. Arf1-GTP-induced tubule formation suggests a function of Arf family proteins in curvature acquisition at sites of vesicle budding. *The Journal of biological chemistry*. 283:27717-27723.

Kreitzer, G., A. Marmorstein, P. Okamoto, R. Vallee, and E. Rodriguez-Boulan. 2000. Kinesin and dynamin are required for post-Golgi transport of a plasma-membrane protein. *Nature cell biology*. 2:125-127.

Lee, W.L., R.E. Harrison, and S. Grinstein. 2003. Phagocytosis by neutrophils. *Microbes and infection / Institut Pasteur*. 5:1299-1306.

Link, T.M., U. Park, B.M. Vonakis, D.M. Raben, M.J. Soloski, and M.J. Caterina. 2010. TRPV2 has a pivotal role in macrophage particle binding and phagocytosis. *Nature immunology*. 11:232-239.

Lippincott-Schwartz, J., L.C. Yuan, J.S. Bonifacino, and R.D. Klausner. 1989. Rapid redistribution of Golgi proteins into the ER in cells treated with brefeldin A: evidence for membrane cycling from Golgi to ER. *Cell*. 56:801-813.

Liu, Y.C., E.R. Chapman, and D.R. Storm. 1991. Targeting of neuromodulin (GAP-43) fusion proteins to growth cones in cultured rat embryonic neurons. *Neuron*. 6:411-420.

Lundqvist-Gustafsson, H., M. Gustafsson, and C. Dahlgren. 2000. Dynamic ca(2+)changes in neutrophil phagosomes A source for intracellular ca(2+)during phagolysosome formation? *Cell calcium*. 27:353-362.

Miller, S.G., L. Carnell, and H.H. Moore. 1992. Post-Golgi membrane traffic: brefeldin A inhibits export from distal Golgi compartments to the cell surface but not recycling. *The Journal of cell biology*. 118:267-283.

Miyake, K., and P.L. McNeil. 1995. Vesicle accumulation and exocytosis at sites of plasma membrane disruption. *The Journal of cell biology*. 131:1737-1745.

Niedergang, F., and P. Chavrier. 2004. Signaling and membrane dynamics during phagocytosis: many roads lead to the phagos(R)ome. *Current opinion in cell biology*. 16:422-428.

Praefcke, G.J., and H.T. McMahon. 2004. The dynamin superfamily: universal membrane tubulation and fission molecules? *Nature reviews. Molecular cell biology*. 5:133-147.

Reddy, A., E.V. Caler, and N.W. Andrews. 2001. Plasma membrane repair is mediated by Ca(2+)-regulated exocytosis of lysosomes. *Cell*. 106:157-169.

Ridley, A.J., M.A. Schwartz, K. Burridge, R.A. Firtel, M.H. Ginsberg, G. Borisy, J.T. Parsons, and A.R. Horwitz. 2003. Cell migration: integrating signals from front to back. *Science*. 302:1704-1709.

Rosa, P., F.A. Barr, J.C. Stinchcombe, C. Binacchi, and W.B. Huttner. 1992. Brefeldin A inhibits the formation of constitutive secretory vesicles and immature secretory granules from the trans-Golgi network. *European journal of cell biology*. 59:265-274.

Samie, M., X. Wang, X. Zhang, A. Goschka, X. Li, X. Cheng, E. Gregg, M. Azar, Y. Zhuo, A.G. Garrity, Q. Gao, S. Slaugenhaupt, J. Pickel, S.N. Zolov, L.S. Weisman, G.M. Lenk, S. Titus, M. Bryant-Genevier, N. Southall, M. Juan, M. Ferrer, and H. Xu. 2013. A TRP channel in the lysosome regulates large particle phagocytosis via focal exocytosis. *Developmental cell*. 26:511-524.

952 Scalettar, B.A., P. Rosa, E. Taverna, M. Francolini, T. Tsuboi, S. Terakawa, S.
953 Koizumi, J. Roder, and A. Jeromin. 2002. Neuronal calcium sensor-1 binds
954 to regulated secretory organelles and functions in basal and stimulated
955 exocytosis in PC12 cells. *Journal of cell science*. 115:2399-2412.
956 Shen, C., S.S. Rathore, H. Yu, D.R. Gulbranson, R. Hua, C. Zhang, N.E. Schoppa, and
957 J. Shen. 2015. The trans-SNARE-regulating function of Munc18-1 is
958 essential to synaptic exocytosis. *Nature communications*. 6:8852.
959 Shui, W., L. Sheu, J. Liu, B. Smart, C.J. Petzold, T.Y. Hsieh, A. Pitcher, J.D. Keasling,
960 and C.R. Bertozzi. 2008. Membrane proteomics of phagosomes suggests a
961 connection to autophagy. *Proceedings of the National Academy of Sciences*
962 *of the United States of America*. 105:16952-16957.
963 Singh, D.K., D. Kumar, Z. Siddiqui, S.K. Basu, V. Kumar, and K.V. Rao. 2005. The
964 strength of receptor signaling is centrally controlled through a
965 cooperative loop between Ca2+ and an oxidant signal. *Cell*. 121:281-293.
966 Sollner, T., S.W. Whiteheart, M. Brunner, H. Erdjument-Bromage, S. Geromanos, P.
967 Tempst, and J.E. Rothman. 1993. SNAP receptors implicated in vesicle
968 targeting and fusion. *Nature*. 362:318-324.
969 Steegmaier, M., J. Klumperman, D.L. Foletti, J.S. Yoo, and R.H. Scheller. 1999.
970 Vesicle-associated membrane protein 4 is implicated in trans-Golgi
971 network vesicle trafficking. *Molecular biology of the cell*. 10:1957-1972.
972 Steinhardt, R.A., G. Bi, and J.M. Alderton. 1994. Cell membrane resealing by a
973 vesicular mechanism similar to neurotransmitter release. *Science*.
974 263:390-393.
975 Stendahl, O., K.H. Krause, J. Krischer, P. Jerstrom, J.M. Theler, R.A. Clark, J.L.
976 Carpentier, and D.P. Lew. 1994. Redistribution of intracellular Ca2+ stores
977 during phagocytosis in human neutrophils. *Science*. 265:1439-1441.
978 Stenmark, H. 2009. Rab GTPases as coordinators of vesicle traffic. *Nature reviews.*
979 *Molecular cell biology*. 10:513-525.
980 Sudhof, T.C. 2012. Calcium control of neurotransmitter release. *Cold Spring*
981 *Harbor perspectives in biology*. 4:a011353.
982 Tardieux, I., P. Webster, J. Ravesloot, W. Boron, J.A. Lunn, J.E. Heuser, and N.W.
983 Andrews. 1992. Lysosome recruitment and fusion are early events
984 required for trypanosome invasion of mammalian cells. *Cell*. 71:1117-
985 1130.
986 Togo, T., J.M. Alderton, G.Q. Bi, and R.A. Steinhardt. 1999. The mechanism of
987 facilitated cell membrane resealing. *Journal of cell science*. 112 (Pt 5):719-
988 731.
989 Togo, T., T.B. Krasieva, and R.A. Steinhardt. 2000. A decrease in membrane
990 tension precedes successful cell-membrane repair. *Molecular biology of*
991 *the cell*. 11:4339-4346.
992 Underhill, D.M., and A. Ozinsky. 2002. Phagocytosis of microbes: complexity in
993 action. *Annual review of immunology*. 20:825-852.
994 Velasco, A., L. Hendricks, K.W. Moremen, D.R. Tulsiani, O. Touster, and M.G.
995 Farquhar. 1993. Cell type-dependent variations in the subcellular
996 distribution of alpha-mannosidase I and II. *The Journal of cell biology*.
997 122:39-51.
998 Vicker, M.G. 1977. On the origin of the phagocytic membrane. *Experimental cell*
999 *research*. 109:127-138.

Vinet, A.F., M. Fukuda, and A. Descoteaux. 2008. The exocytosis regulator synaptotagmin V controls phagocytosis in macrophages. *Journal of immunology*. 181:5289-5295.

Warnock, D.E., T. Baba, and S.L. Schmid. 1997. Ubiquitously expressed dynamin-II has a higher intrinsic GTPase activity and a greater propensity for self-assembly than neuronal dynamin-I. *Molecular biology of the cell*. 8:2553-2562.

Zhang, Q., D. Cox, C.C. Tseng, J.G. Donaldson, and S. Greenberg. 1998. A requirement for ARF6 in Fcgamma receptor-mediated phagocytosis in macrophages. *The Journal of biological chemistry*. 273:19977-19981.

Zuchner, S., M. Noureddine, M. Kennerson, K. Verhoeven, K. Claeys, P. De Jonghe, J. Merory, S.A. Oliveira, M.C. Speer, J.E. Stenger, G. Walizada, D. Zhu, M.A. Pericak-Vance, G. Nicholson, V. Timmerman, and J.M. Vance. 2005. Mutations in the pleckstrin homology domain of dynamin 2 cause dominant intermediate Charcot-Marie-Tooth disease. *Nature genetics*. 37:289-294.

Figure 1

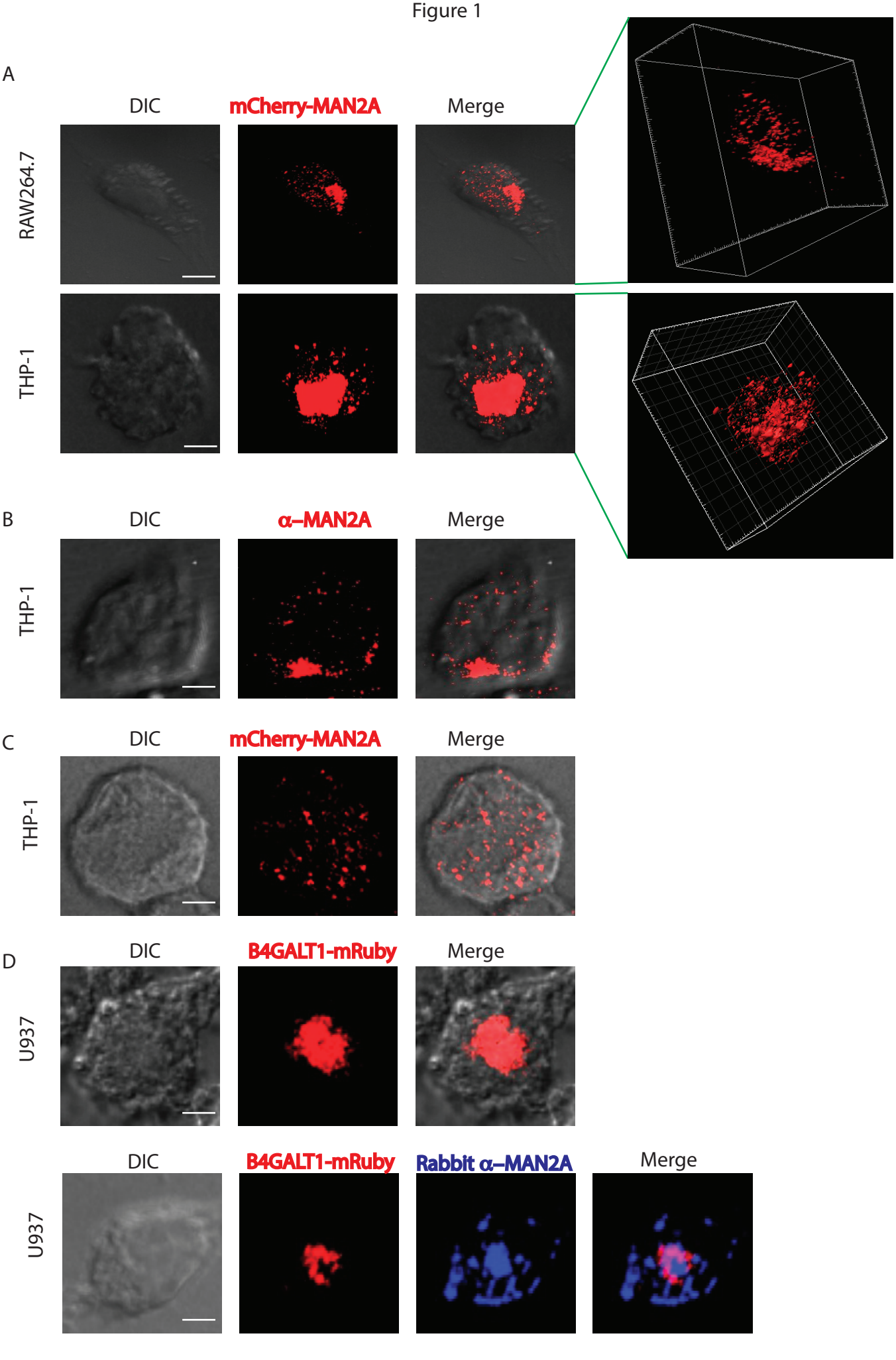

FIGURE LEGENDS

Figure 1: Mannosidase-II is a marker of Golgi apparatus and vesicles derived from the Golgi

A) RAW264.7 cells and THP-1 derived macrophages were nucleofected with mCherry-MAN2A. At 24 hours post nucleofection, cells were visualized under the confocal microscope (see methods for detail). The 3-D plots at the right were created using Imaris 7.2 software tool (scale bar: 5μm).

B) THP-1 derived macrophages were permeabilized using 0.5% TritonX-100 and stained with anti-Mannosidase-II antibody followed by the secondary antibody tagged with Alexa-560, fixed and visualized under the confocal microscope (scale bar: 5μm).

C) THP-1 derived macrophages were nucleofected with mCherry-MAN2A. At 24 hours post nucleofection, the cells were treated with Brefeldin A (20μM) for 4 hours and visualized under the microscope (scale bar: 5μm).

D) U937 human macrophages, stably expressing the Golgi marker mRuby-B4GALT1 (red, β-galactosyl transferase). For the lower panel, B4GALT1 (red) expressing U937 macrophages were stained with anti-Mannosidase-II antibody followed by secondary antibody (Alexa-405, blue, scale bar: 5μm).

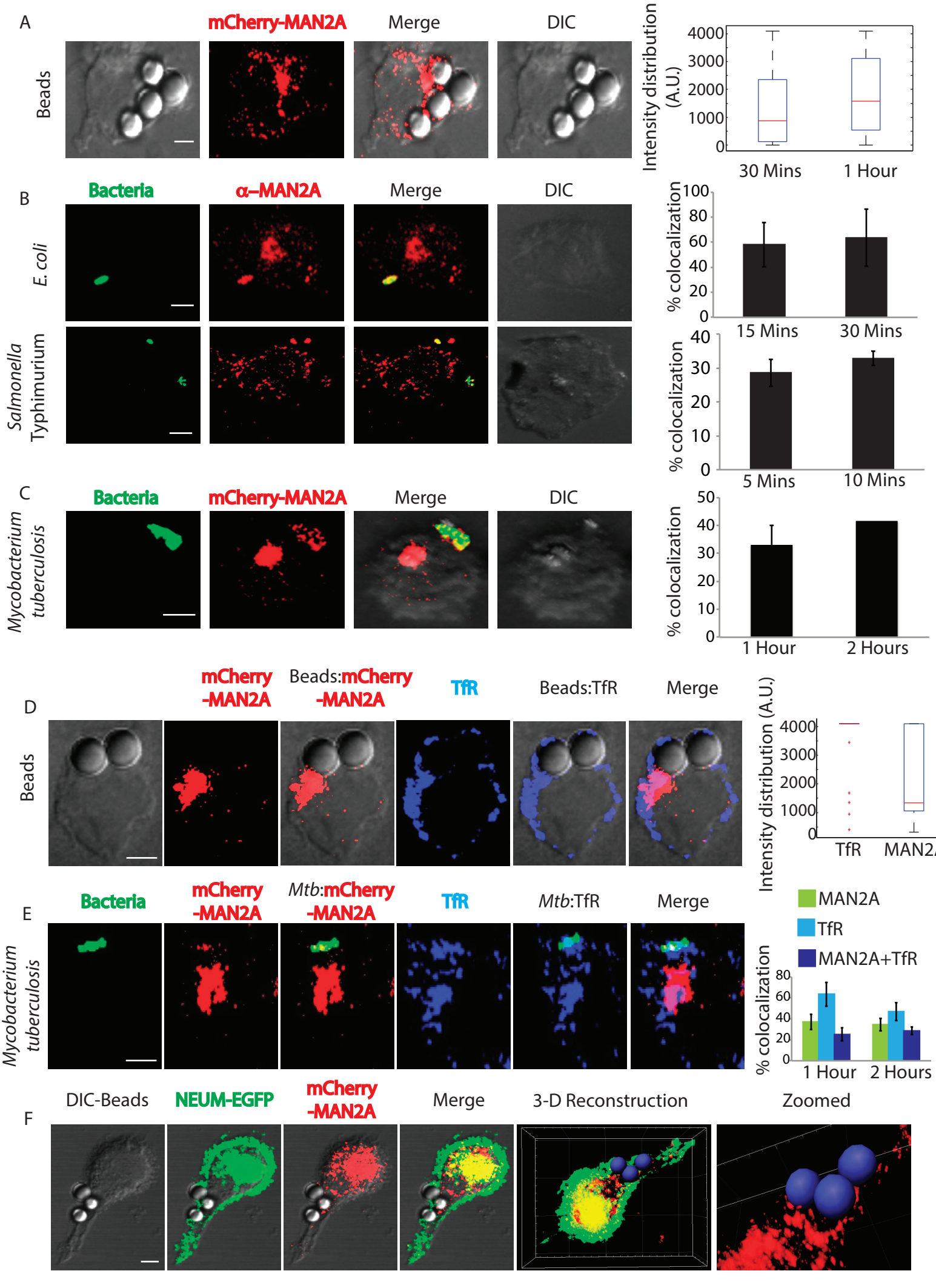

Figure 2: Mannosidase-II is recruited at the site of phagocytosis

A) RAW264.7 macrophages expressing mCherry-MAN2A (red) were incubated with mouse-IgG coated latex beads for 30 minutes and 1 hour. The images shown are representative from the 30 minutes samples. At the right, the total intensity of mCherry-MAN2A puncta on the bead surface was estimated using 3D spot creation module in Imaris 7.2 and the intensity distribution of the population has been plotted (see methods for detail). The box plot represents data from more than 200 beads analyzed from two different experiments (values ± S.D.; scale bar: 4μm).

B) THP-1 derived macrophages were infected with PKH67 labeled *E. coli* (green, top panel) or GFP expressing *Salmonella* Typhimurium (green, lower panel) for 15 and 30 minutes. Cells were then stained with anti-Mannosidase-II antibody followed by Alexa 568 tagged secondary antibody (red). Images shown are representative from the 15 minutes samples from both the experiments. The bar plots at the right show % co-localization of *E. coli* or *Salmonella* with Mannosidase-II at the surface at 5 and 10 or 15 and 30 minutes respectively post-infection. Data represents average of more than 200 bacteria from two different experiments (values ± S.D.; scale bar: 3μm).

C) mCherry-MAN2A (red) expressing THP-1 derived macrophages were infected with PKH67 labeled H37Rv (green) for 1 and 2 hours. Samples were fixed and visualized under the microscope. The bar-plot at the right shows % co-localization of H37Rv with Mannosidase-II at both these time points. Data represents average of more than 200 bacteria from two different experiments (values ± S.D.; scale bar: 4μm).

D) mCherry-MAN2A (red) expressing RAW264.7 macrophages were incubated with mouse-IgG coated latex beads for 30 minutes or 1 hour. At the respective time points, cells were immune-stained with anti-TfR antibody followed by a secondary

antibody tagged with Alexa 405 (blue). Presence of TfR or Mannosidase-II at the bead surface was calculated in terms of fluorescence intensity using the 3D spot creation module in Imaris 7.2software. The box-plot at the right shows data from more than 100 beads from two independent experiments (scale bar: 5μm).

E) mCherry-MAN2A (red) expressing RAW264.7 macrophages were infected with PKH67 labeled H37Rv (green) for 1 and 2 hours. At the respective time points, samples were fixed and stained with anti-Transferrin receptor antibody followed by Alexa-405 tagged secondary antibody (blue). The images are representative from the 1 hour time point. For the plots at the right, % co-localization of H37Rv with Mannosidase-II, TfR or both Mannosidase-II and TfR was calculated using Imaris 7.2. The data represents average of more than 150 bacteria from three different experiments (values ± S.D.; scale bar: 5μm).

F) U937 cells stably expressing EGFP (green) at the plasma-membrane using a membrane targeting tag from Neuromodulin (NEUM-EGFP) were nucleofected with mCherry-MAN2A (red) and incubated with human-IgG coated latex beads for 30 minutes. The 3-D constructions at the right hand side were performed using 3D spot creation module in Imaris 7.2 to visualize the juxtaposition of Mannosidase-II and latex beads against the plasma membrane (scale bar: 5μm).

Figure 3

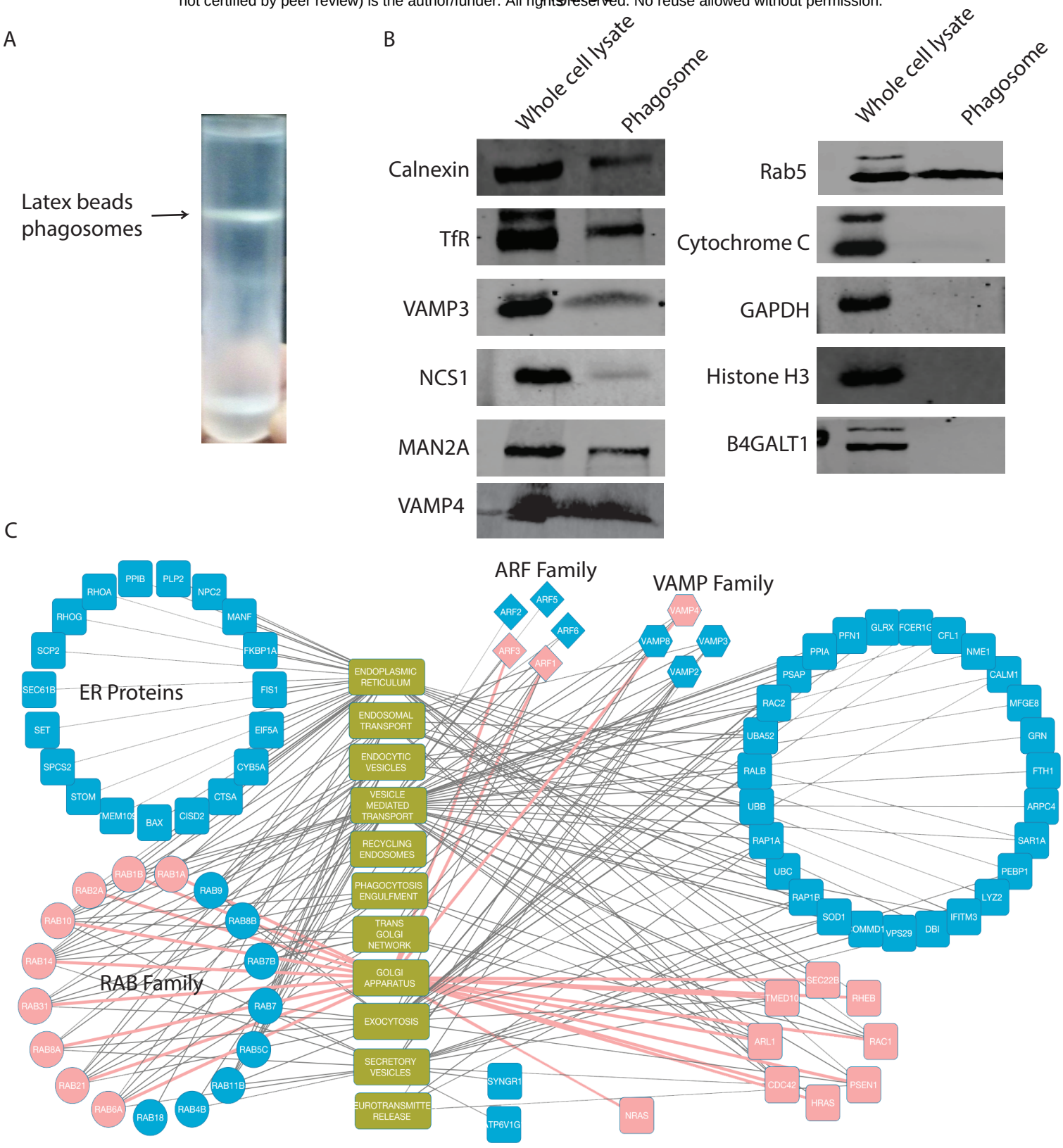

Figure 3: Proteomic analysis reveals presence of several VAMPs, ARFs and RABs in the early phagosomes

A) Preparation of latex bead phagosomes from THP-1 derived macrophages on a sucrose density gradient (see methods)

B) THP-1 derived macrophages were incubated with latex beads (1μm size) for 1 hour. Phagosomes were isolated using differential density ultracentrifugation and samples were probed for indicated markers using Western blots.

C) Latex beads phagosomes isolated from RAW264.7 macrophages were lysed and resolved on a 10% SDS-PAGE (Fig. S2). The lane below 25kDa molecular weight was analyzed using mass spectrometry to identify enrichment of low molecular weight proteins (see methods). The list of genes identified was then searched in the AMIGO2.0 database to establish functional association. Finally the representative network was constructed using Cytoscape 2.6.1. The pink nodes and edges in the network denote association with the Golgi apparatus.

Figure 4

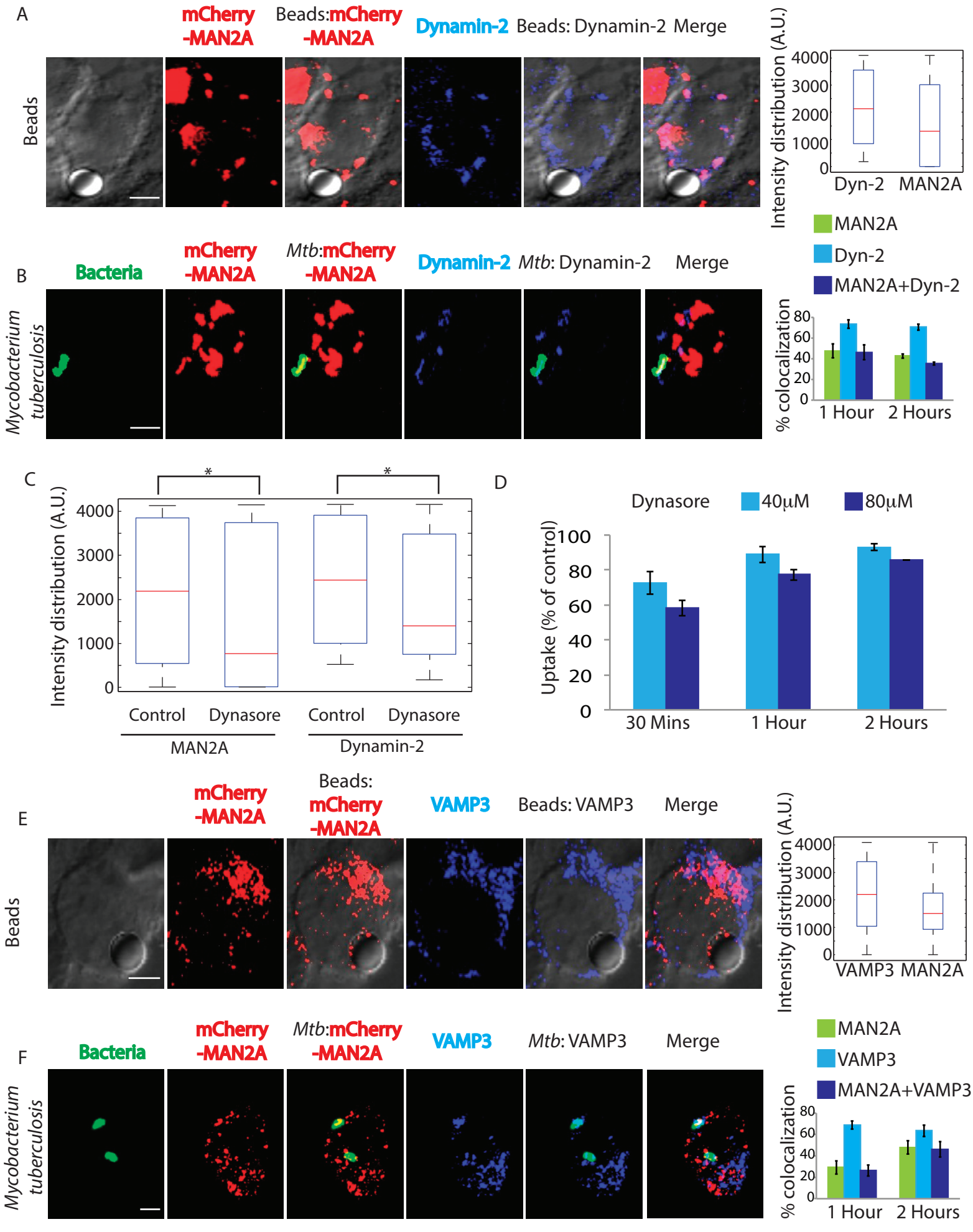

Figure 4: Golgi-derived vesicles are recruited through focal exocytosis

A) mCherry-MAN2A (red) expressing RAW264.7 macrophages were incubated with mouse-IgG coated latex beads for 30 minutes or 1 hour. At the respective time points, cells were immune-stained with anti-dynamin2 antibody followed by a secondary antibody tagged with Alexa 405 (blue). Presence of dynamin2 (Dyn-2) or Mannosidase-II at the bead surface was calculated using the Imaris 7.2 software. The box-plot at the right shows data from more than 100 beads from two independent experiments (values ± S.D.; scale bar: 4μm).

B) mCherry-MAN2A (red) expressing THP-1 macrophages were infected with PKH67 labeled H37Rv (green) for 1 and 2 hours. At the respective time points, samples were fixed and stained with anti-dynamin2 antibody followed by Alexa-405 tagged secondary antibody (blue). The images are representative from the 1hour time point. For the plots at the right, % co-localization of H37Rv with Mannosidase-II, dynamin2 or both Mannosidase-II and dynamin2 was calculated using Imaris 7.2. The data represents average of more than 150 bacteria from three different experiments (values ± S.D.; scale bar: 4μm).

C) mCherry-MAN2A (red) expressing RAW264.7 macrophages were pretreated with 80μM Dynasore and incubated with mouse-IgG coated latex beads for 30 minutes or 1 hour. At 30 minutes, samples were fixed and stained with anti-dynamin2 antibody followed by Alexa-405 tagged secondary antibody (blue). Intensity of Mannosidase-II and dynamin at the bead surface was calculated using the 3D spot creation module in Imaris 7.2 software. The box-plot shows data from more than 100 beads from two independent experiments (*p-value<0.05).

D) THP 1 derived macrophages were treated with the respective dynasore concentrations for 4 hours and incubated with FITC labeled latex beads (1μm). At the

respective time points cells were fixed and analyzed by flow cytometry. To calculate % uptake, data for each cargo for a given time point, the dynasore treated set was normalized against the respective untreated control set (values ± S.D.).

E) mCherry-MAN2A (red) expressing RAW264.7 macrophages were incubated with mouse-IgG coated latex beads for 30 minutes or 1 hour. At the respective time points, cells were immune-stained with anti-VAMP-3 antibody followed by a secondary antibody tagged with Alexa 405 (blue). Presence of VAMP-3 or Mannosidase-II at the bead surface was calculated using the 3D spot creation module in Imaris 7.2 software. The box-plot at the right shows data from more than 100 beads from two independent experiments (scale bar: 5μm).

F) mCherry-MAN2A (red) expressing THP-1 derived macrophages were infected with PKH67 labeled H37Rv (green) for 1 and 2 hours. At the respective time points, samples were fixed and stained with anti-VAMP-3 antibody followed by Alexa-405 tagged secondary antibody (blue). The images are representative from the 1hour time point. For the plots at the right, % co-localization of H37Rv with Mannosidase-II, VAMP-3 or both Mannosidase-II and VAMP-3 was calculated using Imaris 7.2. The data represents average of more than 150 bacteria from three different experiments (values ± S.D.; scale bar: 4μm).

Figure 3

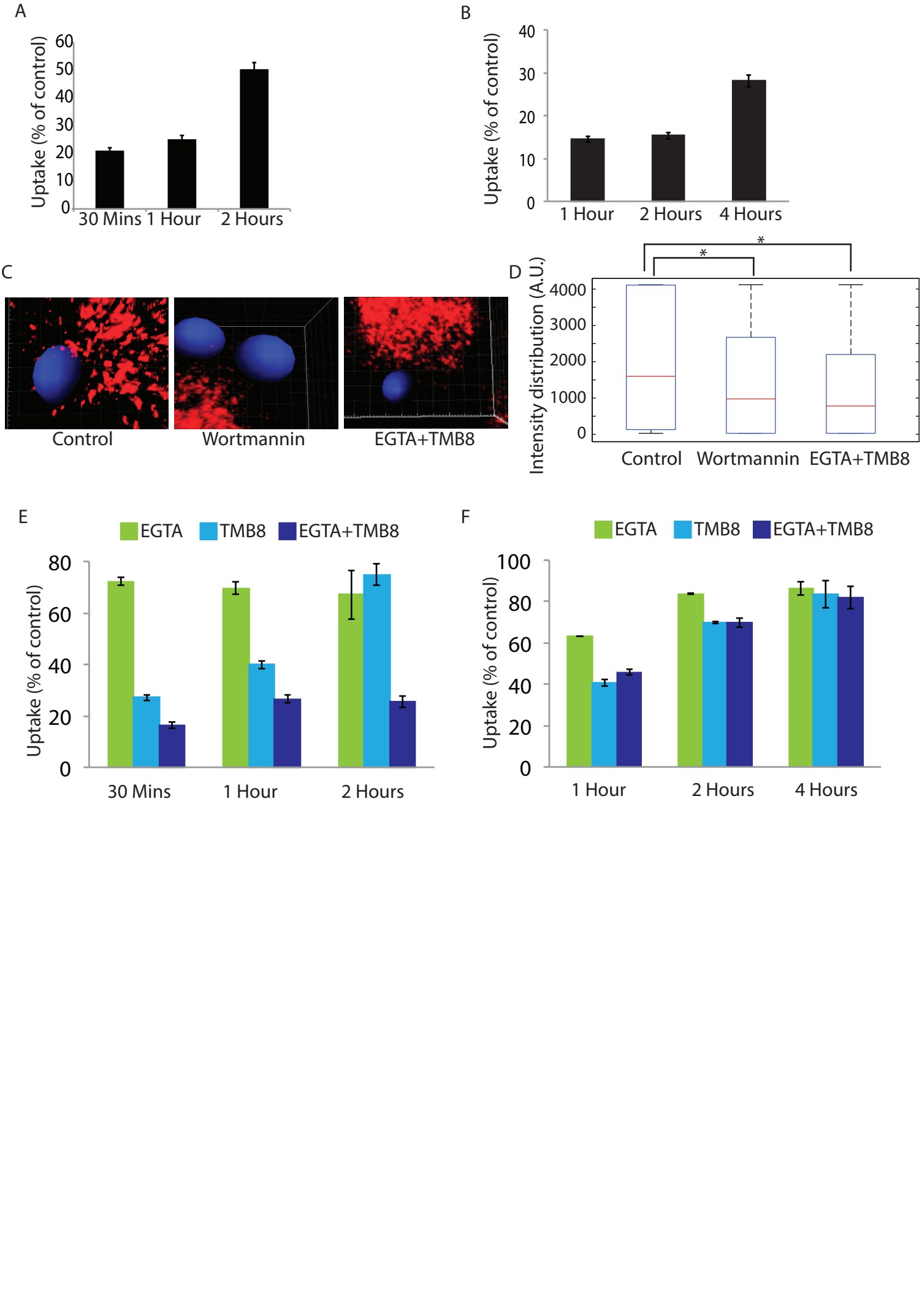

Figure 5: Role of PIP3 and Calcium from intra and extra-cellular sources in recruitment of Mannosidase II vesicles:

A) THP-1 derived macrophages were pre-treated with 5µM wortmannin for 4 hours. FITC latex beads (1µm) were added to these. The cells were fixed at respective time points and analyzed by flow cytometry. Data shown are average from three different experiments and represented as % uptake in treated cells with respect to the untreated cells (values ± S.D.).

B) THP-1 derived macrophages were pre-treated with 5µM wortmannin for 4 hours. They were infected with PKH labeled H37Rv. At respective time points the cells were fixed and analyzed by flow cytomtery**.** Data shown are average from three different experiments and represented as % uptake in treated cells with respect to the untreated cells (values ± S.D.).

C) mCherry-MAN2A (red) expressing RAW264.7 macrophages were pre-treated with 5µM Wortmannin or EGTA (3mM)+TMB8 (100 µM) for 30 minutes respectively. The cells were incubated with mouse-IgG coated latex beads for 30 minutes or 1 hour. At the respective time points, cells were fixed and analyzed by confocal microscopy. The images shown are representative from the 30 minutes samples. The 3D construction of latex bead was done using spot creation module of Imaris 7.2.

D) RAW264.7 macrophages expressing mCherry-MAN2A (red) were incubated with mouse-IgG coated latex beads for 30 minutes and 1 hour. The total intensity of mCherry-MAN2A puncta on the bead surface was determined using 3D spot creation module in Imaris 7.2 and the intensity distribution of the population has been plotted. The box plot represents data from more than 200 beads analyzed from two different experiments (*p-value<0.05).

E) THP-1 derived macrophages were pre-treated with EGTA (3mM), TMB8 (100µM) and EGTA+TMB8 for 30 minutes before addition of FITC latex beads (1µm). At respective time points the cells were fixed and analyzed by flow cytometry. Data shown are average from three different experiments and represented as % uptake in treated cells with respect to the untreated cells (values ± S.D.).

F) THP-1 derived macrophages were pre-treated with EGTA (3mM), TMB8 (100µM) and EGTA+TMB8 for 30 minutes before addition of PKH labeled H37Rv. At respective time points the cells were fixed and analyzed by flow cytometry. Data shown are average from three different experiments and represented as % uptake in treated cells with respect to the untreated cells (values ± S.D.).

Figure 6

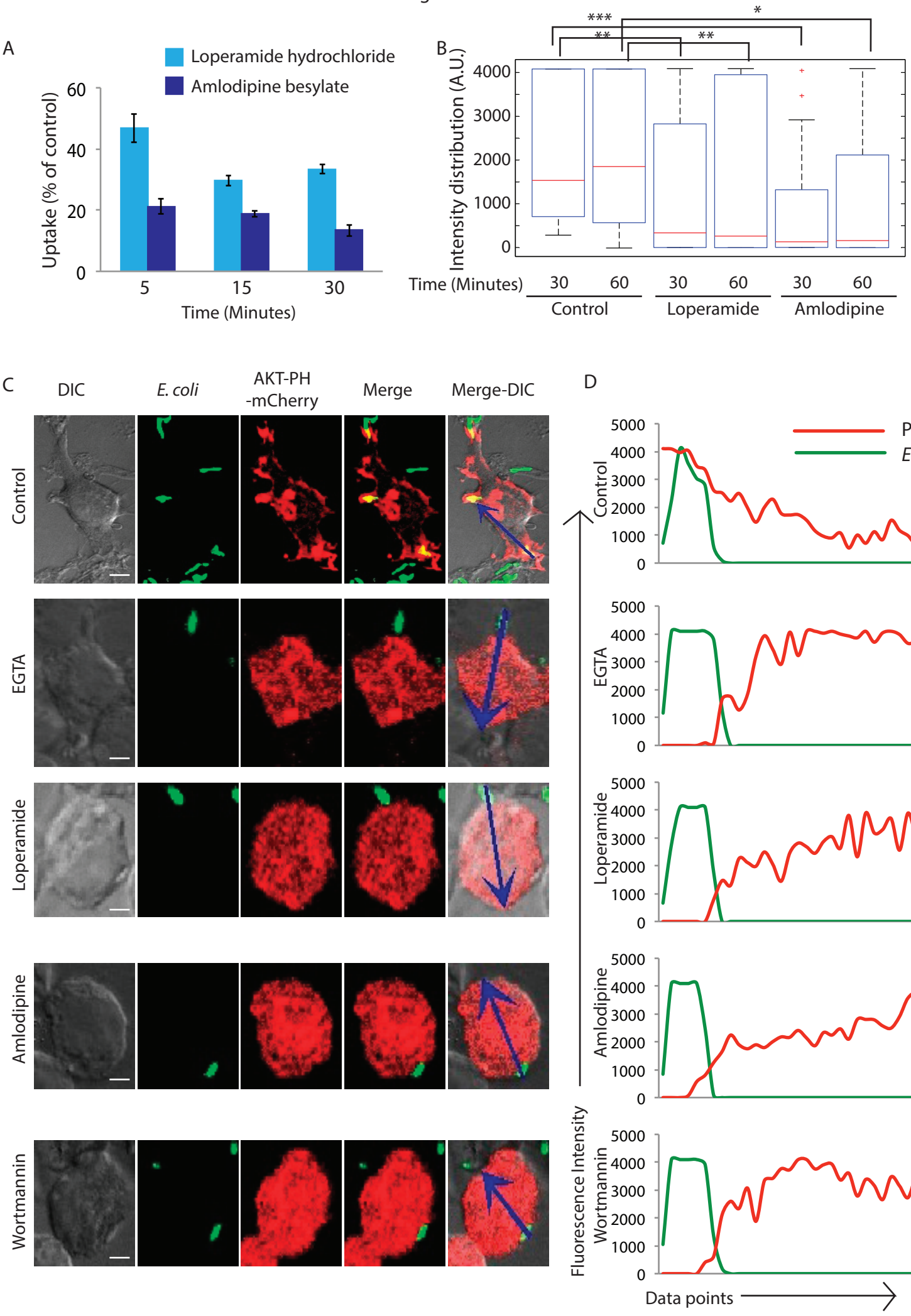

Figure 6: Ca^{2+} entry through voltage-gated Ca^{2+} channel helps establish PIP3 gradient to aid phagocytosis

A) THP-1 derived macrophages were pre-treated with Amlodipine (100µM) or Loperamide (100µM) for 30 minutes before addition of GFP expressing *E. coli*. At respective time points the cells were fixed and analyzed by flow cytometry**.** Data shown are average from three different experiments and represented as % uptake in the treated cells with respect to the untreated cells (values ± S.D.).

B) RAW264.7 macrophages expressing mCherry-MAN2A (red) were pre-treated with amlodipine (100µM) or loperamide (100µM) for 30 minutes and subsequently incubated with mouse-IgG coated latex beads for 30 minutes and 1 hour. The total intensity of mCherry-MAN2A puncta on the bead surface was determined using 3D spot creation module in Imaris 7.2 and the intensity distribution of the population has been plotted. The box-plot represents data from more than 200 beads analyzed from two different experiments (*p-value<0.05, **p-value<0.01 and ***p-value<0.005).

C) RAW264.7 macrophages were transfected with AKT-PH-mCherry. At 24 hours of cells were incubated with GFP expressing E coli for 5 minutes. In parallel we also had AKT-PH-mCherry expressing cells that were pre-treated with EGTA (3mM), loperamide (100µM), amlodipine (100µM) or wortmannin (5uM) followed by incubation with GFP expressing *E. coli* for 5 minutes. Samples were fixed at 5 minutes and analyzed by confocal microscopy. The arrows in the extreme right image in each of the panel highlight the fluorescence intensity measurements for the analysis presented in figure 6D (scale bar: 4µm).

D) Images in figure 6C (arrows) were analyzed using intensity profile line tool in the NIS-elements software (see methods). The data represent median from more than 20 fields for each case.

Figure 7

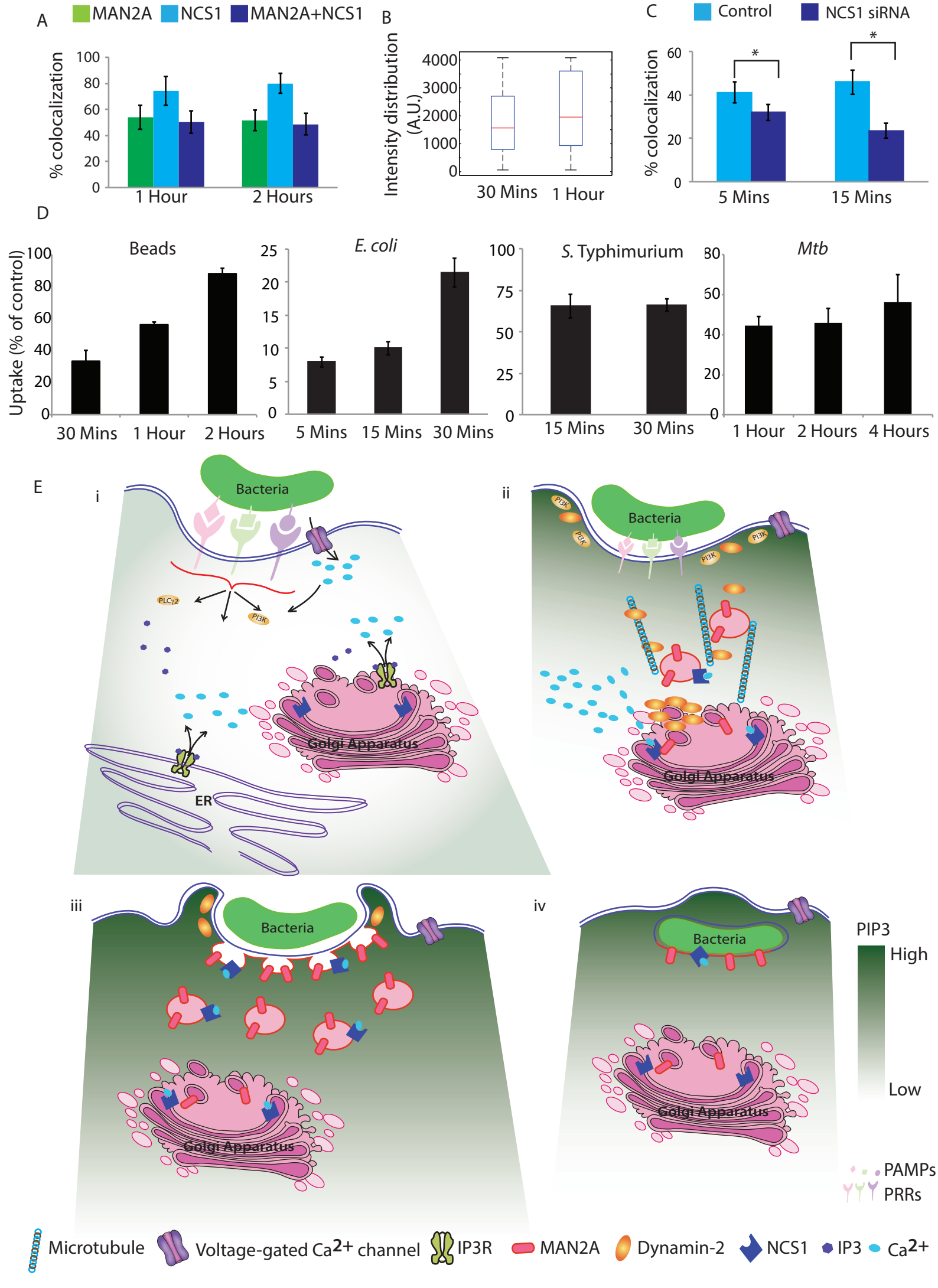

Figure 7: The neuronal calcium sensor (NCS1) in the Golgi apparatus recognizes Ca2+ signal for focal release of Mannosidase-II vesicles

A) mCherry-MAN2A (red) expressing U937 derived macrophages were infected with PKH67 labeled H37Rv (green) for 1 and 2 hours. At the respective time points, samples were fixed and stained with anti-NCS1 antibody followed by Alexa-405 tagged secondary antibody. The images are representative from the 1hour time point. Percent co-localization of H37Rv with Mannosidase-II, NCS1 or both Mannosidase-II and NCS1 was calculated using Imaris 7.2. The data represents average of more than 150 bacteria from three different experiments (values ± S.D.).

B) In U937 macrophages, incubated with beads for 30 minutes or 1 hour, samples were stained with anti-NCS1 antibody. Presence of NCS1 at the bead surface was calculated using the 3D spot creation module in Imaris 7.2 software. The box-plot at the right shows data from more than 100 beads from two independent experiments.

C) THP-1 derived macrophages treated with NCS1 siRNA were incubated with GFP expressing *E. coli* for 5 and 15 minutes. Cells were stained with anti-Mannosidase-II antibody to assess the recruitment of Mannosidase-II at the phagosomes in NCS1 depleted cells. The total intensity of mCherry-MAN2A puncta on the E coli surface was determined using 3D spot creation module in Imaris 7.2. For lower panel, percent co-localization of *E. coli* with Mannosidase-II was calculated using Imaris 7.2. The data represents average of more than 150 bacteria from three different experiments (values ± S.E.M, *p-value<0.05; scale bar: 2μm).

D) THP-1 macrophages were treated with siRNA against NCS1 or scrambled control. At 48 hours post siRNA treatment, cells were monitored to uptake latex beads (1μm), *E coli*, *Salmonella* Typhimurium. or H37Rv for indicated time points. Data are shown as % uptake in the siRNA treated cells with respect to the scrambled siRNA

control treated cells. Data are representative of three independent experiments (values ± S.D.).

E) A model to explain the Ca2+ dependent activation of NCS1 to trigger the focal movement of Golgi derived vesicles. i) Initial recognition of an object (bacteria, beads, cell debris etc) for phagocytosis results in membrane depolarization possibly due to torsional stress and resulting in the activation of voltage gated Ca^{2+} channels, leading to the entry of extracellular Ca^{2+} into the cells. The entry of $Ca2^{+}$ through voltage-gated Ca^{2+} channels sets the focus for quick and efficient recruitment of PI3K and results in the accumulation of PIP3 at the site of phagocytosis. These early events are further aided by signaling through specific pattern recognition receptors and release of Ca^{2+} from intracellular stores. ii) Increased cytosolic Ca^{2+} is sensed by Golgi-resident NCS1, which triggers the movement of Mannosidase-II vesicles towards the site of phagocytosis, guided by a gradient of PIP3, along with dynamin and microtubule. iii) Mannosidase-II vesicles fuse with the membrane at the site of phagocytosis and help grow the phagosome around the cargo before final scission and internalization. iv) The membrane of the nascent phagosome is contributed in part by the plasma membrane and rest from the Golgi-derived vesicles (in this model for clarity, we have excluded lysosome and recycling endosomes as additional sources, see text).